JHEP

Published for SISSA by Springer

Received: September 16, 2021
Accepted: November 13, 2021
Published: November 23, 2021

Sensitivity to BSM effects in the Higgs p_T spectrum within SMEFT

Marco Battaglia,[a] **Massimiliano Grazzini,**[b] **Michael Spira**[c] **and Marius Wiesemann**[d]

[a] *Santa Cruz Institute for Particle Physics, University of California Santa Cruz, Santa Cruz, CA 95064, U.S.A.*
[b] *Physik Institut, Universität Zürich, CH-8057 Zürich, Switzerland*
[c] *Paul Scherrer Institut, CH-5232 Villigen PSI, Switzerland*
[d] *Max-Planck-Institut für Physik, 80805 München, DE-80805 Germany*

E-mail: marco.battaglia@ucsc.edu, grazzini@physik.uzh.ch, Michael.Spira@psi.ch, wieseman@mpp.mpg.de

Abstract: The study of Higgs boson production at large transverse momentum is one of the new frontiers for the LHC Higgs physics programme. This paper considers boosted Higgs production in the Standard Model Effective Field Theory (SMEFT). We focus on the gluon fusion and $t\bar{t}H$ production processes and study the effects of three dimension-6 operators: the top Yukawa operator, the gluon-Higgs effective coupling and the chromo-magnetic dipole operator of the top quark. We perform a detailed study of the sensitivity of current and future LHC data to the corresponding Wilson coefficients, consistently accounting for their renormalisation group evolution. We compare the sensitivities obtained with only linear and linear + quadratic terms in the SMEFT by using the spectrum shape and the addition of the Higgs signal yields. We also consider fits of p_T spectra in models with heavy-top partners and in MSSM scenarios with a light scalar top and study the validity of the SMEFT assumptions as a function of the new-particle masses and the Higgs p_T range. Finally, we extract constraints on the Wilson coefficients for gluon fusion from a simultaneous fit to the ATLAS and CMS data and compare our results with those obtained in global SMEFT analyses.

Keywords: Beyond Standard Model, Hadron-Hadron scattering (experiments), Higgs physics

ArXiv ePrint: 2109.02987

https://doi.org/10.1007/JHEP11(2021)173

Contents

JHEP11(2021)173

1 Introduction

After the discovery of the scalar resonance with a mass of 125 GeV [1, 2] the study of its properties has been one of the main activities of the LHC physics programme. The measurements carried out up to now have shown that, within the current accuracy, the new resonance has properties compatible with those predicted for the Higgs boson in the Standard Model (SM) and no significant deviations from the SM picture emerged so far.

At the theoretical level there are two major options to explore scenarios beyond the SM (BSM): either by introducing extensions of the SM particle content through explicit BSM models, or by parametrising deviations from the SM picture supplementing the Lagrangian with higher-dimensional operators built from SM fields. With the assumption that new physics fulfils the decoupling theorem [3], the effect of these operators is suppressed by powers of the new-physics scale Λ [4–7]. The scale Λ might be a heavy new-particle mass or a combination thereof, if there are several new particles beyond the SM. This approach is model independent and, when combined with the SM gauge symmetries, it defines the SM Effective Field Theory (SMEFT) (see ref. [8] for a review).[1]

[1] An even more general approach is the one in which the $SU(2)_L \otimes U(1)$ gauge symmetry is assumed to be realised non linearly and the Higgs field is introduced as scalar singlet. This is the so called Higgs EFT (HEFT) (see e.g. [9–14]), and can be used to deal with non-decoupling BSM scenarios.

A number of SMEFT studies have been carried out in the Higgs sector in recent years, and a considerable amount of work has been devoted to develop appropriate tools to include dimension-six operators [15–20]. SMEFT analyses including a broad range of measurements, in the Higgs sector and beyond, have been presented in refs. [21–29].

The amount of data collected at the LHC in Run 2 and the perspectives for Run 3 and the High Luminosity programme (HL-LHC) offer the possibility to study the *dynamical* properties of the Higgs boson in different kinematic regimes. This is achieved by analyzing Higgs processes involving a large momentum scale inside the relevant matrix element. Of particular interest is the region in which the Higgs boson is produced at large transverse momentum. Measurements in this region shed light on the structure of the interactions of the Higgs boson with strongly interacting particles and might unveil BSM effects that are not revealed through inclusive measurements.

Higgs boson production at large transverse momentum resolves the structure of the Higgs coupling to gluons and possible BSM effects are modeled within SMEFT through effective operators that modify the shape of the spectrum. The SMEFT approach does not specify the UV completion and has a finite range of validity in the Higgs transverse momentum (p_T^H) which depends on the scale Λ. On the other hand, if the experimental accuracy at large p_T^H is not sufficient, the measurements will not be sensitive to effects originating from the detailed nature of the UV-completion. Conversely, the theoretical accuracy of the SM cross section will also limit the BSM sensitivity of these measurements. The (universal) interpretation in terms of SMEFT Wilson coefficients will in addition be limited by the theoretical precision of SMEFT effects beyond the SM, and, therefore, the consistent inclusion of higher-order corrections to SMEFT contributions is also relevant [30].

The total Higgs-production cross section in the dominant production channel, namely gluon fusion (ggF), is not sufficient to resolve all combinations of the dimension-6 Wilson coefficients. Only with the inclusion of additional production modes, such as the associated production with a top-antitop pair ($t\bar{t}H$), and by considering more exclusive observables, such as differential cross sections, it is possible to disentangle the effects of the relevant dimension-6 operators. The Higgs transverse-momentum distribution and its shape are particularly sensitive to different combinations of the Wilson coefficients at large transverse momentum.

The ATLAS and CMS collaborations have already reported measurements of the Higgs transverse-momentum spectrum [31–34] from the analysis of the full LHC Run 2 data. They have also presented dedicated boosted $H \to b\bar{b}$ analyses aiming to access Higgs production at large transverse momentum [35–37]. This provides us with a first set of experimental data to analyse and renders it possible to obtain rather accurate projections of the experimental uncertainties on the Higgs transverse-momentum spectrum in measurements throughout the LHC programme up to the HL-LHC [38, 39].

The leading order (LO) transverse-momentum distribution of the Higgs boson in ggF production is known since long time including the full quark-mass dependence [40, 41]. The NLO QCD corrections have first been obtained in the heavy-top-limit (HTL) and have the effect of increasing the differential cross section by roughly a factor of two [42–45]. At NLO, finite top-mass effects have been estimated in terms of a large top-mass expansion [46, 47].

JHEP11(2021)173

They have later been supplemented by the inclusion of the full top-mass dependence in the real corrections [48, 49]. Further improvements of the virtual contribution were obtained in refs. [50, 51] through the use of an asymptotic expansion. The exact NLO QCD calculation has eventually been completed in ref. [52] through the numerical integration of the corresponding two-loop diagrams. The next-to-next-to-leading order (NNLO) QCD corrections have been determined in the HTL leading to a moderate increase of the differential cross section and a significant reduction of the residual scale dependence [53–55]. The NLO and approximate NNLO theoretical predictions at high-p_T have been combined in ref. [56] and compared with the predictions from the other production channels and with the predictions of commonly used event generators [49, 57–59]. The transverse momentum spectrum involving additional dimension-6 (and dimension-8) operators has been studied in refs. [60–70].

In this paper Higgs boson production at large p_T^H is studied in the framework of SMEFT. Neglecting the bottom- and charm-loop contributions, which are irrelevant at large transverse momentum, we focus on three operators: a point-like coupling of the Higgs boson to gluons, a modification of the top-quark Yukawa coupling and the chromomagnetic dipole operator, that modifies the coupling between gluons and the top quark, with and without the Higgs boson at the same vertex. As far as the gluon fusion channel is concerned, the calculation including the effects of these operators has been performed in refs. [64–66]. Besides gluon fusion, the $t\bar{t}H$ channel is also sensitive to the same operators and, at large p_T, gives a non-negligible contribution in the experimental analyses. Therefore, we have included this production mode in our study, by carrying out the corresponding calculation in SMEFT. For the other production modes, that are not affected by the above operators, we just stick to the SM predictions.

The central goal of the present study is to place bounds on the relevant Wilson coefficients of the dimension-6 operators from current LHC data and to assess the sensitivity on those Wilson coefficients that can be reached in the remainder of the LHC programme. To this end, we exploit a calculation of the p_T spectrum in SMEFT in combination with available state-of-the-art SM predictions [56] for all the relevant channels, and we perform multi-parameter fits of the deviations from the SM transverse-momentum spectrum modelled by the Wilson coefficients that can be resolved within the experimental and theoretical uncertainties. In this context, we also compare our results with those obtained with analyses in the top sector [71], in particular for the chromomagnetic dipole operator. Constraints from the present results are obtained with a simultaneous EFT fit to the preliminary ATLAS and the CMS data.

In our analysis we probe scales from the Higgs mass up to 1 TeV, and it is therefore important to consistently include the renormalisation group evolution of the Wilson coefficients. This is done by solving the corresponding RG equations [72–74] at leading-logarithmic (LL) accuracy.

Since the experimental sensitivity is approaching p_T^H values of order of 1 TeV, it becomes mandatory to assess the validity range of the EFT fits at the upper end of the Higgs transverse-momentum spectrum when extracting information on explicit models. We perform such study by fitting the p_T^H spectra in a new-physics model with a heavy top partner

JHEP11(2021)173

and in MSSM-like scenarios with a light scalar top through a linear and a non-linear EFT expansion of the dimension-6 operators. We then compare, as a function of the upper value of the p_T^H fit range, the values of the Wilson coefficients extracted from our fits to those obtained by matching the explicit models to the EFT when integrating out the heavy degrees of freedom.

The paper is organised as follows. In section 2 we introduce the theoretical framework and the calculations on which our analysis is based. Section 3 describes the methodology of the EFT fits, and section 4 discusses the range of validity of the EFTs. In section 5 we report the extraction of the Wilson coefficients, we assess the sensitivity that can be reached through the LHC programme and the constraints that can be derived with the current LHC data. Section 6 gives our conclusions. The appendix is devoted to the discussion and solution of the renormalisation group equations for the Wilson coefficients.

2 Theoretical framework

In the SMEFT the full set of 2499 dimension-6 operators built from SM fields is added to the SM Lagrangian:

$$\mathcal{L}_{\text{eff}} = \mathcal{L}_{\text{SM}} + \sum_i \frac{c_i}{\Lambda^2}\mathcal{O}_i\,, \tag{2.1}$$

where Λ denotes the scale of new physics, $\mathcal{O}_i$ are the dimension-6 operators and c_i the corresponding Wilson coefficients. Neglecting the bottom- and charm-loop contributions,[2] which have no impact at large p_T, the following three operators are relevant for our study of the transverse-momentum distribution of the Higgs boson in gluon fusion:

$$\begin{aligned}
\mathcal{O}_1 &= |H|^2 G^a_{\mu\nu} G^{a,\mu\nu}\,,\\
\mathcal{O}_2 &= |H|^2 \bar{Q}_L H^c t_R + h.c.\,,\\
\mathcal{O}_3 &= \bar{Q}_L H \sigma^{\mu\nu} T^a t_R G^a_{\mu\nu} + h.c.\,,
\end{aligned} \tag{2.2}$$

which, for single-Higgs production, can be expanded as:

$$\begin{aligned}
\frac{c_1}{\Lambda^2}\,\mathcal{O}_1 &\to \frac{\alpha_s}{\pi v} c_g h G^a_{\mu\nu} G^{a,\mu\nu}\,,\\
\frac{c_2}{\Lambda^2}\,\mathcal{O}_2 &\to \frac{m_t}{v}(1-c_t) h\bar{t}t\,,\\
\frac{c_3}{\Lambda^2}\,\mathcal{O}_3 &\to c_{tg}\frac{g_S m_t}{2v^3}(v+h) G^a_{\mu\nu}(\bar{t}_L \sigma^{\mu\nu} T^a t_R + h.c)\,,
\end{aligned} \tag{2.3}$$

with $\sigma^{\mu\nu} = \frac{i}{2}[\gamma^\mu, \gamma^\nu]$ and $G^a_{\mu\nu} = \partial_\nu G^a_\mu - \partial_\mu G^a_\nu + g_s f_{abc} G^b_\mu G^c_\nu$. The operator $\mathcal{O}_1$ describes a point-like contact interaction between the Higgs boson and gluons, the operator $\mathcal{O}_2$ corresponds to a modification of the top Yukawa coupling and the operator $\mathcal{O}_3$ denotes the chromomagnetic dipole operator that modifies the coupling between gluons and the top quark, with and without the Higgs boson at the same vertex.

[2] Modifications of the bottom and charm Yukawa coupling have a significant impact only at small transverse momenta of the Higgs boson in gluon fusion, while the bottom Yukawa can be accessed also via the $b\bar{b}H$ production mode [75–81], and through the decay $H \to b\bar{b}$.

JHEP11(2021)173

At large transverse momenta, the p_T^H spectrum receives contributions from several production modes. For the ggF contribution we employ our calculation of the p_T^H spectrum presented in ref. [65], which we have implemented in the numerical program MoRe-HqT. With More-HqT the transverse-momentum spectrum at small p_T is evaluated at next-to-leading-logarithmic (NLL) accuracy and matched to the LO result at high p_T, while being NLO accurate for the cumulative cross section in p_T, so as to achieve NLL+NLO accuracy. The program MoRe-HqT is based on the MoRe-SusHi code [82–84], which computes the NLL+NLO p_T spectrum in the SM with full quark-mass dependence [82] and in models with extended Higgs sectors, in particular a simple 2-Higgs Doublet Model, in the MSSM [83], or in the NMSSM [84]. The contribution of the chromomagnetic operator O_3 has also been implemented [66]. For the resummed contribution at small p_T^H the program relies on the b-space implementation of the HqT code [85, 86]. In the present study we focus on the large-p_T^H region, where the spectrum is effectively described at LO, but with the inclusion of all relevant dimension-6 operators.

The Wilson coefficients are scale dependent quantities and they obey renormalization group equations (RGEs) [72–74]. We have solved such RGEs at LL accuracy and consistently included the result in our calculation. The complete derivation is outlined in appendix A. The solutions read

$$
\begin{aligned}
c_t(Q^2) &= c_t(\mu_0^2) + \frac{24}{5}\,\frac{m_t^2(\mu_0^2)}{v^2}\,c_{tg}(\mu_0^2)\,\left\{\left(\frac{\alpha_s(Q^2)}{\alpha_s(\mu_0^2)}\right)^{\frac{5}{6\beta_0}} - 1\right\}\,,\\
c_{tg}(Q^2) &= c_{tg}(\mu_0^2)\left(\frac{\alpha_s(Q^2)}{\alpha_s(\mu_0^2)}\right)^{-\frac{7}{6\beta_0}}\,,\\
c_g(Q^2) &= \frac{\beta_0+\beta_1\alpha_s(Q^2)/\pi}{\beta_0+\beta_1\alpha_s(\mu_0^2)/\pi}\left\{c_g(\mu_0^2) - \frac{3\pi}{5-6\beta_0}\,\frac{m_t^2(\mu_0^2)}{v^2}\,\frac{c_{tg}(\mu_0^2)}{\alpha_s(\mu_0^2)}\left[\left(\frac{\alpha_s(Q^2)}{\alpha_s(\mu_0^2)}\right)^{\frac{5}{6\beta_0}-1} - 1\right]\right\},
\end{aligned}
\tag{2.4}
$$

where μ_0 is the input scale at which the Wilson coefficients are extracted and Q is the actual dynamical scale at which the operators are evaluated for a given process, that we identify with the renormalization scale μ_R of the strong coupling constant, α_s, of the process. We evaluate eq. (2.4) following the same strategy as outlined in ref. [87]. In particular, that means that the $\overline{\text{MS}}$ mass of the top quark at the scale μ_0, $m_t(\mu_0^2)$, is evaluated by converting the on-shell top mass to $m_t(m_t)$ with the 4-loop expression of ref. [88] and then evolving with 4-loop running to $m_t(\mu_0^2)$ [89, 90]. For α_s, on the other hand, we use the 2-loop running as given by the employed set of parton densities.

Since the same effective operators also enter the $t\bar{t}H$ production mode, which has a non-negligible contribution to the transverse-momentum spectrum of the Higgs boson at large p_T, we compute the transverse-momentum spectrum with the inclusion of the dimension-6 operators of eq. (2.3). We have performed this calculation both analytically and by using MadGraph5_aMC@NLO [91]. For the latter the generation of the relevant matrix elements has been carried out by using as input the `SMEFTatNLO` Unified FeynRules Output

JHEP11(2021)173

(UFO) model [20]. The MadGraph5_aMC@NLO results for $t\bar{t}H$ production have been compared with our independent analytical calculation finding complete agreement.[3] The translation of the MadGraph5_aMC@NLO conventions for the Wilson coefficients into our notation is derived through[4]

$$\begin{aligned} \texttt{cpG} &= \frac{\alpha_s}{\pi}\,\frac{\Lambda^2}{v^2}\,c_g\,, \\ \texttt{ctp} &= \frac{\sqrt{2}m_t}{v}\,\frac{\Lambda^2}{v^2}\,(1-c_t)\,, \\ \texttt{ctG} &= \frac{m_t}{\sqrt{2}v}\,\frac{\Lambda^2}{v^2}\,c_{tg}\,. \end{aligned} \tag{2.5}$$

Since we set the scale of the operators to be equal to the renormalization scale μ_R, this translation has to be carried out at the scale μ_R used in the $t\bar{t}H$ calculation. Moreover, given that the factor $\sqrt{2}\,m_t/v$ originates from the Yukawa coupling, whose renormalization is on-shell in the $t\bar{t}H$ calculation, we set m_t to the value of the pole mass in the conversion of eq. (2.5). This ensures that, disregarding running effects, c_t remains a rescaling of the SM Yukawa coupling. Finally, we include the running of the Wilson coefficients also in the $t\bar{t}H$ calculation by evolving the operators from the input scale μ_0 to μ_R through eq. (2.4) before converting to the MadGraph5_aMC@NLO conventions with eq. (2.5).

The chromomagnetic dipole operator is of particular interest because it can be tested also in the top sector [71, 92]. The corresponding Wilson coefficient C_{tG} of these works is related to our c_{tg} as

$$\frac{C_{tG}}{\Lambda^2} = c_{tg}\frac{g_s\,m_t}{\sqrt{2}v^3}\,. \tag{2.6}$$

In eq. (2.6) the scale of $g_s = \sqrt{4\pi\alpha_s}$, of the $\overline{\text{MS}}$ top mass m_t and of the Wilson coefficients should be understood as m_t. To the best of our understanding, in the analyses of [71, 92] the running of the Wilson coefficients is neglected and the scale Λ is set to 1 TeV. In this work we include the effect of the QCD running as discussed above. When the transverse momenta span over a large range (for instance for the p_T^H spectrum from $\mathcal{O}(100)$ GeV to 1–2 TeV), it is essential to include the QCD running of the Wilson coefficients in order to consistently perform an EFT analysis.

Our computations of the high-p_T^H cross section in gluon fusion and in $t\bar{t}H$ production are used to obtain the BSM effects as ratios of the Higgs cross section with SMEFT corrections, $\sigma_i(c_t, c_g, c_{tg})$, to the SM prediction, σ_i^{SM}:

$$R_i(c_g, c_{tg}, c_t) = \Delta\sigma_i(c_t, c_g, c_{tg})/\Delta\sigma_i^{\text{SM}}\,, \tag{2.7}$$

where $\Delta\sigma_i$ is the differential cross section integrated in each p_T^H bin i and both numerator

[3] We note that with MadGraph5_aMC@NLO the $t\bar{t}H$ calculation could in principle be carried out at NLO. However, since the computation for the ggF process can only be performed at LO, and, moreover, the $t\bar{t}H$ contribution is subdominant, we limit ourselves to use our LO result.

[4] The advantage of our convention is explicitly visible in the simplicity of the RGEs derived in appendix A, i.e. the leading effects of the QCD running are factorized in terms of the α_s and m_t factors that lead to a pure BSM evolution of our coefficients c_t, c_g, c_{tg} at LL level, if c_{tg} does not vanish at the input scale.

JHEP11(2021)173

and denominator are computed at the same order in perturbation theory. These ratios, computed on a grid of values of c_g, c_{tg} and c_t, are employed to study the potential of Higgs measurements at large p_T^H to constrain the effects of the dimension-6 operators.

We specify the parameters used for all predictions obtained in the remainder of this paper. We use the five-flavour scheme with the corresponding NLO set of the PDF4LHC2015 [93–98] parton distribution functions (PDFs) and the respective value of the strong coupling constant. The top-quark pole mass is set to 172.5 GeV. Since the $R_i(c_g, c_{tg}, c_t)$ ratios are computed in the LO approximation, they are independent of the overall powers of the QCD coupling α_s and their respective setting of the renormalisation scale μ_R. We also find that they are largely independent of the choice of the factorisation scale μ_F, since the parton densities approximately cancel in the ratio, and they also show only a mild dependence on the scale at which the Wilson coefficients are evaluated, which we also choose as μ_R. We evaluate the ratios R_i in eq. (2.7) by dynamically setting $\mu_R = \mu_F = m_T$, where m_T denotes the transverse mass of the Higgs boson $m_T = \sqrt{m_H^2 + p_{TH}^2}$, for the ggF process. In the case of $t\bar{t}H$ production the scales are set to $\mu_R = \mu_F = (m_H + 2\,m_t)/2$.

We stress that the choice of a dynamic scale together with eq. (2.4) implies that even though c_g and $c_t - 1$ may vanish at the input scale μ_0, a non-zero value is generated by c_{tg} through their running to the scale Q that depends on the bin in p_T^H under consideration. As a result, c_t is not a simple rescaling of the Higgs cross section, but its running renders it dependent on p_T^H and therefore it will also affect the shape of the Higgs transverse-momentum spectrum, although the effect should be subleading. This also implies that in every given bin in p_T^H, the values of c_g, c_t and c_{tg} differ, and that what we extract in our fits are the Wilson coefficients at the input scale, namely $c_g(\mu_0)$, $c_t(\mu_0)$ and $c_{tg}(\mu_0)$. In order to obtain the Wilson coefficients at any other scale we may again employ their evolution in eq. (2.4). This is completely analogous to the treatment of the strong coupling constant α_s in its measurements or to simultaneous extractions of α_s and the top-quark mass m_t, where their QCD running is a crucial consistency aspect of the respective template fits. We also stress that our definition of the dimension-6 operators in eq. (2.3) is particularly convenient, as it expresses the running of the operators by the one of α_s and m_t, and limits the mixing terms to contributions induced by c_{tg}.

3 Fitting the Higgs p_T spectrum

The Wilson coefficients c_g, c_{tg} and c_t are extracted from the Higgs p_T spectrum by using a multi-parameter fit of the predicted deviations $R_i(c_g, c_{tg}, c_t)$ for each bin i in p_T^H to the ratio of the measured cross section over the best SM prediction in each bin, while taking into account the experimental and theoretical uncertainties. To compute $R_i(c_g, c_{tg}, c_t)$ we have generated the Higgs transverse-momentum spectra for ggF production with MoRe-HqT on a three dimensional grid for $-1.0 \leq c_g \leq 1.0$, $-0.5 \leq c_{tg} \leq 0.5$, and $0.1 \leq c_t \leq 2.0$, and on bins of 50 GeV in the Higgs transverse momentum. The range in c_g and c_{tg} is chosen according to the sensitivity of the current dataset. Similarly, the p_T^H spectra for $t\bar{t}H$ production have been generated with MadGraph5_aMC@NLO, after translating

JHEP11(2021)173

the Wilson coefficients to the conventions used in our study at the scale μ_R and including their running from μ_0 to μ_R, see eq. (2.5) and eq. (2.4), respectively. In order to match the binning of the experimental measurements the p_T^H spectra are rebinned by integrating the cross section values for the chosen bin interval and normalising to the bin width. After rebinning, the values $R_i(c_g, c_{tg}, c_t)$ are calculated separately for each production mode (ggF and/or $t\bar{t}H$) by taking the ratio to the corresponding SM cross sections evaluated with the same tools (i.e. at the same order in perturbation theory). The maps, which are defined as the EFT spectra for all values of the Wilson coefficients, are stored for each production process as sets of ROOT [99] histograms.

The fitting code is based on the MINUIT package [100] in the ROOT framework. Histograms in the map of the EFT spectra generated for a specific scan are loaded in the fitting program as vectors of histograms, whose index is related to the (c_g, c_{tg}, c_t) values used to generate them. Each map of the EFT spectra has a reference SM spectrum used to compute the R_i values. The spectrum that is fitted can be chosen to be one of the histograms stored in the EFT scan maps, as a histogram from a benchmark model or as the signal strength values reported by the LHC experiments.

The fitting procedure minimizes the χ^2 of the fit with respect to the values of the Wilson coefficients. Since the grid of the Wilson coefficients used for the EFT scans is discrete, the R_i values for arbitrary combinations of (c_g, c_{tg}, c_t) within the ranges given above are evaluated in the fitting code by an interpolation between the two closest generated values. When performing fits to the p_T^H spectrum including the contribution of both ggF and $t\bar{t}H$ production modes the χ^2 is evaluated from the sum of the ggF and $t\bar{t}H$ EFT contributions, each weighted by the assumed fractions f_{ggF}, $f_{t\bar{t}H}$ of signal events in the sample. What remains is a SM-like spectrum with a fraction $1 - f_{ggF} - f_{t\bar{t}H}$ for the VH and VBF production modes that is not sensitive to the $\mathcal{O}_1$, $\mathcal{O}_2$ and $\mathcal{O}_3$ EFT operators.

The fit has three free parameters: c_g and c_{tg}, defined at μ_0=125 GeV unless stated otherwise, and an overall normalisation factor, approximately corresponding to c_t^2, that can be fitted to remove the sensitivity to the integrated cross section. Alternatively, this sensitivity can also be removed by normalising the R_i values to the average R computed in a p_T range below the lower edge of the fit region. The fitting procedure has been extensively validated by generating benchmark ratios R_i of the p_T^H spectra for various combinations of (c_g, c_{tg}, c_t) within the given parameter space normalised to the reference SM spectrum and comparing the ensuing fitted values of (c_g, c_{tg}) to the input used to generate them. An example of a fitted benchmark spectrum is shown in figure 1, which clearly shows that the fit reproduces the benchmark spectrum and the input values (c_g, c_{tg})=(0.01, 0.01) are precisely returned by the fit, yielding $c_g = 0.01 \pm 0.04$ and c_{tg}=0.01±0.10, where the quoted uncertainties are correlated and simply result from the assumed errors on the benchmark spectrum.

3.1 Comparing EFT effects in ggF and $t\bar{t}H$ production

The ggF and $t\bar{t}H$ production modes are sensitive to the same dimension-6 EFT operators. Moreover, at high p_T^H the relative contribution of the $t\bar{t}H$ process increases and a considerable fraction of $t\bar{t}H$ events are accepted alongside ggF events by the selection criteria

JHEP11(2021)173

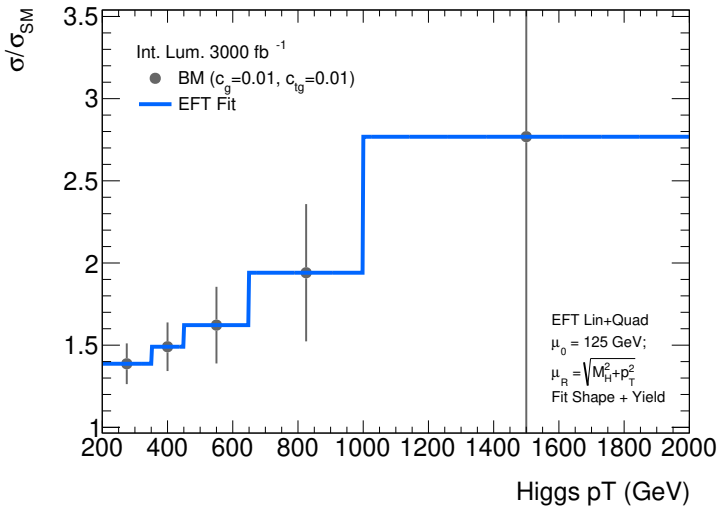

Figure 1. Example of an EFT fit on a benchmark p_T^H spectrum (pseudo data) with the binning adopted by the experiments. The R_i deviations from the SM values for the ($c_g(M_H) = 0.01$, $c_{tg}(M_H) = 0.01$, $c_t(M_H) = 1.0$) benchmark spectrum are given by the points with the estimated bin-by-bin uncertainties, which are obtained by combining the predicted ATLAS and CMS accuracies with 12% uncertainty on the SM cross section, while the continuous line shows the result of the EFT fit.

applied in the boosted analyses inclusive over the production modes. The ATLAS collaboration reports that $\simeq 15\%$ of the signal events selected at $p_T > 650\,\text{GeV}$ originate from $t\bar{t}H$ production [37]. In view of this, it is important to evaluate the EFT effects on the p_T^H spectrum for the Wilson coefficients[5] c_g, c_{tg} for both ggF and $t\bar{t}H$ events. We compare those effects by computing the R_i ratios in 2-dimensional c_g, c_{tg} scan for ggF and $t\bar{t}H$ production separately.

Here we focus on the situation in which both linear and quadratic terms are added in the EFT expansion. When only linear terms are considered the weight of $t\bar{t}H$ production is found to be significantly smaller. Figure 2 shows the ratio of $R_i \times f$ for ggF to the one for $t\bar{t}H$ in three different p_T^H bins, where f is the typical fraction of signal events for the respective production mode accepted in the ATLAS and CMS analyses. Qualitatively, the pattern of enhancement at high p_T^H is similar for the two production processes. This seems to exclude the possibility of cancellation effects due to opposing contributions from ggF and $t\bar{t}H$. Quantitatively, the effects of the gluon-fusion production process are dominant over the parameter space with the exception of the region with c_g values close to zero, where the enhancement of the ggF process becomes relatively small. In this region, the effects from ggF and $t\bar{t}H$ production are comparable when taking into account the difference in the signal-event fractions f, as we do in our analysis. Large values of c_{tg}, which would correspond to a large enhancement of EFT effects in the $t\bar{t}H$ channel, are excluded by precision measurements in the top sector [71], as indicated by the blue-shaded area in the plots. In combination with the larger fractions of ggF-produced Higgs bosons

[5]The scaling of the ggF and $t\bar{t}H$ cross section with c_t^2 is straightforward, since we only include top-quark loops in the ggF cross section.

JHEP11(2021)173

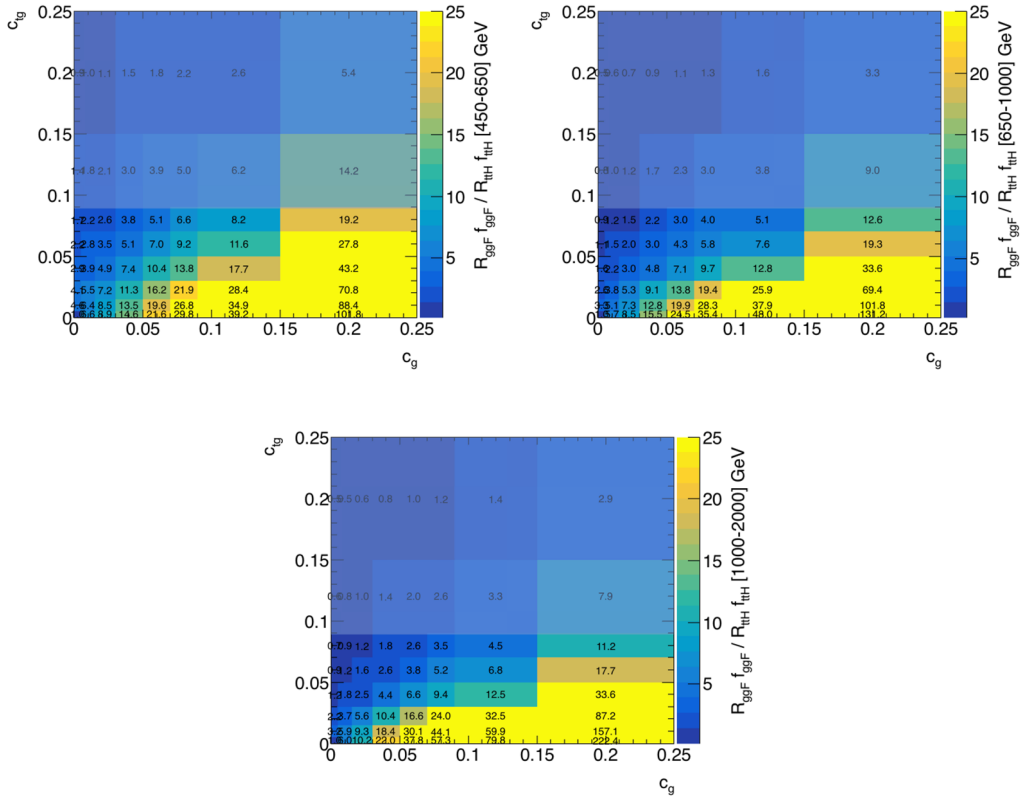

Figure 2. Ratios of EFT yields normalised to SM predictions in the ggF to $t\bar{t}H$ production processes in the intervals $450 < p_T^H < 650\,\text{GeV}$ (top left), $650 < p_T^H < 1000\,\text{GeV}$ (top right) and $1000 < p_T^H < 2000\,\text{GeV}$ (bottom center), weighted by the signal fractions f_{ggF}=0.50 and $f_{t\bar{t}H}$=0.15 of ggF and $t\bar{t}H$ accepted signal events, respectively, corresponding to the values reported for the ATLAS and CMS analyses. The blue shaded area indicates the range of c_{tg} values excluded by the fit of top observables of ref. [71] translated to our definition of $c_{tg}(\mu_0)$ for $\mu_0 = 125\,\text{GeV}$.

selected by the experimental analyses, this bound ensures that ggF dominates the effects that can be detected at the LHC in boosted Higgs production with the current accuracy. However, $t\bar{t}H$ contributions cannot be neglected as the experimental accuracy will improve. A quantitative assessment is presented in section 5.3.

Another aspect that needs to be taken into account in the interpretation of the experimental data are the different shapes of the p_T^H spectra for the ggF, $t\bar{t}H$, VH and VBF production modes, in particular at their high end of the p_T^H range. As an example, a SM p_T^H spectrum, consisting of 85% ggF and 15% VH production, yields a c_{tg}value of 0.005, if fitted as pure ggF. While this is not yet a concern at the current level of experimental accuracy, the accuracy in the determination of the contribution of the Higgs production processes to the signal sample will become relevant in the study of HL-LHC data, and the VH and VBF production modes should be properly subtracted when extracting the Wilson coefficients under consideration, as we do in our study.

JHEP11(2021)173

4 Validity range of the SMEFT

The application of the SMEFT framework assumes that all the New Physics degrees of freedom can be integrated out. This assumption becomes questionable as the LHC analyses start probing transverse-momentum scales of the order of 1 TeV, requiring to reconsider the SMEFT validity and the possible implications on explicit BSM models. The problem of the breakdown of the SMEFT framework when studying Higgs production has been already considered in several studies, e.g. in refs. [61, 101]. Here, we want to revisit this problem by considering two explicit models of New Physics impacting the shape of the p_T^H spectrum at high values, a heavy top partner model and a MSSM-like model with a light scalar top, and profit from our fitting procedure to draw quantitative conclusions. First, we compute the matching between the explicit models and the SMEFT Wilson coefficients. Both the heavy top partner model and the MSSM-like model with a light scalar top modify only the c_g and c_t Wilson coefficients and do not generate c_{tg} terms at leading order. This also implies that c_g and c_t do not run at LL-level, while c_g does include NLL running through α_s. Then, we study the shape of the p_T^H spectrum in these models, i.e. the R_i correction to the SM, while varying the masses of the relevant particles, and compare them to those in the SMEFT for the c_g and c_t values computed from the matching. Finally, we perform SMEFT fits to these p_T^H spectra and study the fitted value of c_g while changing the upper end of the p_T^H range used in the fit. The fits are performed using the same p_T^H binning adopted for the published experimental studies, assuming a flat relative accuracy of 5% on all the bins, given the small values of the matched Wilson coefficients. This accuracy, whose value is arbitrary and is not meant to reproduce the experimental and theoretical uncertainties, is chosen to ensure that differences of the results obtained while changing the fit range are significant. The comparison of the c_g values from these fits to those obtained via the matching calculation gives quantitative information on the breakdown of the SMEFT approach as a function of the new particle masses and p_T^H fit range.

4.1 Heavy top partner

Several SM extensions predict vector-like quarks, i.e. strongly interacting fermions whose left and right-handed components transform in the same way under the $\mathrm{SU}(2)\otimes\mathrm{U}(1)$ gauge group. These fermions can have different $\mathrm{SU}(2)_L$ quantum numbers: in a singlet (T) or (B), in doublets (T, B), in triplets (X, T, B), but they are in the fundamental representation of the colour SU(3) as the ordinary quarks. The effective Lagrangian describing the interaction of the heavy fermions with SM fields contains a Yukawa interaction between new and SM fermions, which induces a mixing between them whose detailed structure depends on the model [102]. Limits on vector-like partners of third-generation quarks from LHC searches are in the 1.3–1.4 TeV range, depending on the scenario under consideration (see e.g. ref. [103]). The mixing with SM fermions leads to strong constraints from precision EW data [104]. In particular, heavy quark partners contribute to the S and T oblique parameters [105] through mixing. The mass matrices can be diagonalised by suitable biunitary transformations characterised by angles θ_R and θ_L (which are not independent).

JHEP11(2021)173

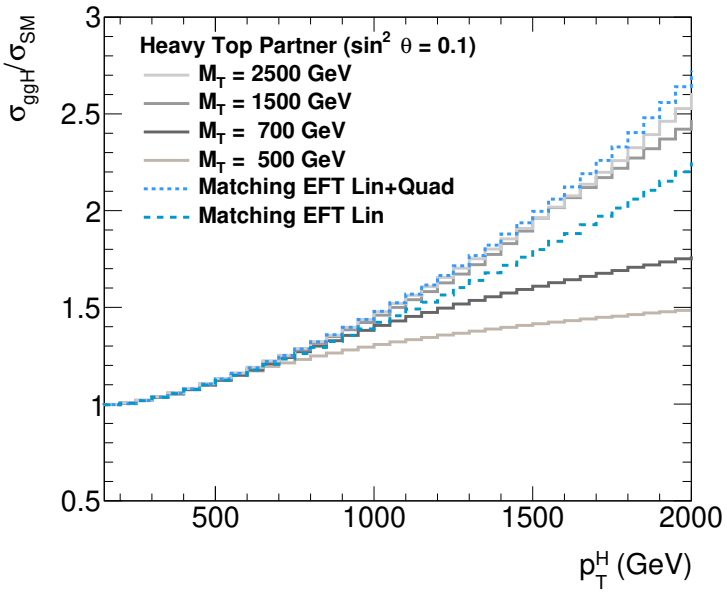

Figure 3. p_T^H spectra normalised to the SM prediction for the heavy top partner model with $M_T = 500$, 700, 1500, 2500 GeV and $\sin^2\theta = 0.1$. The SMEFT spectra for the matched Wilson coefficients and only linear (dashed) and linear plus quadratic (dotted line) terms are also shown.

In the following we consider a simplified model with a top partner with mass M_T. The Yukawa couplings in the top sector can be parametrised in terms of a mixing angle θ and read

$$y_t = \sqrt{2}\,\frac{m_t}{v}\cos^2\theta \qquad y_T = \sqrt{2}\,\frac{M_T}{v}\sin^2\theta\,. \tag{4.1}$$

In the limit $M_T \to \infty$ the top partner can be integrated out and the model is matched to the SMEFT with the following Wilson coefficients:

$$\begin{aligned} c_g &= \frac{\sin^2\theta}{12}\,, \\ c_t &= \cos^2\theta\,, \\ c_{tg} &= 0. \end{aligned} \tag{4.2}$$

In the following, we consider four M_T mass values: 500, 700, 1500, 2500 GeV with $\sin^2\theta$ mixing of 0.1, chosen close to the current experimental limits.

The p_T^H spectra are generated with the MoRe-HqT program. The model spectra, normalised to the SM prediction, are shown in figure 3, compared to the SMEFT spectrum for the matched values of $c_g = 0.1/12 \approx 0.0083$ and $c_t = 0.90$. Qualitatively, the matched SMEFT spectrum reproduces that of the model up to $p_T^H \lesssim M_T$ while at higher p_T^H values, where the model spectrum depends explicitly on M_T^2 mass terms, the SMEFT description breaks down. The patterns observed here correspond to those reported in refs. [61, 106].

The c_g values corresponding to these spectra are extracted by performing SMEFT fits to the p_T^H spectra in the heavy top partner model for the chosen values of M_T. The fits are performed on a p_T^H range from 200 GeV up to an upper limit ranging from 450 GeV

JHEP11(2021)173

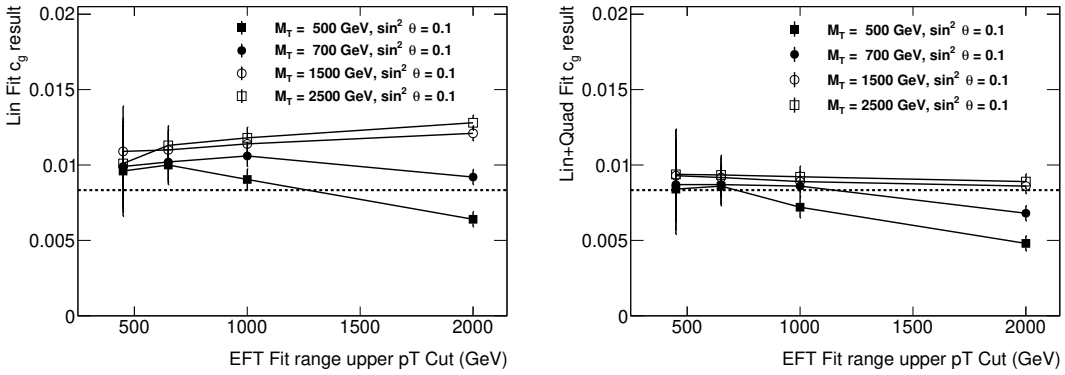

Figure 4. Wilson coefficient c_g values obtained in the SMEFT fit with only linear (left) and with linear plus quadratic terms (right) to p_T^H spectra produced from heavy top partner models with different M_T values and $\sin^2\theta$=0.1 as a function of the upper end of the p_T^H fit range. The dashed lines show the c_g values of the SMEFT matching to the model.

to 2 TeV. The fitted c_g values are shown in figure 4 as a function of the upper limit of the fit range for both linear terms and linear plus quadratic terms included in the SMEFT expansion. In the latter case, the results show that the c_g values obtained from the SMEFT fits agree with the matched values as long as the upper end of the p_T^H range used in the fit is not significantly larger than the heavy top partner mass M_T in the model. When the p_T^H range of the fit overlaps with the value of M_T in the model and probes the p_T^H region where the SMEFT description breaks down, the fitted c_g values drop below the matched value becoming incompatible with it. This marks the breakdown of the SMEFT to describe the heavy top partner model and it is caused by the mismatch between the spectrum in this model and that from the SMEFT when the fit extends to $p_T^H \gtrsim M_T$ values. Therefore, the p_T^H spectrum is not only sensitive to the size of the couplings c_t, c_g, but also to the heavy top-partner mass M_T, if the accessible p_T^H values exceed the value of M_T. In the case of the linear SMEFT fit the situation is different. The fitted c_g values have an upward trend with increasing values of the upper bound of the p_T^H fit range, modulated by the effect of the SMEFT breakdown for $p_T^H \gtrsim M_T$, and they do not reproduce the expected value obtained from the matching calculation.

This result is in line with the different behavior of the spectra obtained by matching with only linear or linear plus quadratic terms in figure 3. In conclusion, the SMEFT expansion with linear and quadratic terms leads to more consistent constraints on the explicit model, as long the p_T^H range is sufficiently small compared to M_T, than when only the linear terms are kept in the SMEFT expansion. This is a clear argument for including quadratic terms in SMEFT fits, which corresponds to an SMEFT expansion at the level of the amplitudes. On the other hand, the question arises if, in that case, dimension-8 operators should not be included as well, the effects of which are of the same order within the SMEFT expansion at the level of the differential cross section. However, dimension-8 operators decouple with the heavy top-partner mass explicitly, since they constitute the first subleading order of an expansion in the inverse of the heavy top-partner mass at the amplitude level. Thus, the quadratic terms of the dimension-6 operators are dominant.

JHEP11(2021)173

Parameter	Benchmark $m_{\tilde{t}}$ 500	Benchmark $m_{\tilde{t}}$ 700	Benchmark $m_{\tilde{t}}$ 1500
$m_{\tilde{t}_1}$ (GeV)	512	712	1572
$m_{\tilde{t}_2}$ (GeV)	2023	2033	2068
$m_{\tilde{b}_1}$ (GeV)	1015	1031	1082
$m_{\tilde{b}_2}$ (GeV)	2017	2027	2059
$\tan\beta$	3.9	3.9	3.9
μ (TeV)	-3.0	-3.0	-3.0
A_t (GeV)	200	200	200
m_{A^0} (TeV)	2.5	2.5	2.5

Table 1. Main parameters of the MSSM-like benchmark scenarios used in the SMEFT validity study.

4.2 MSSM-like scenario with a light scalar top

The second model we consider is a MSSM-like model with a light scalar top quark (stop), $\tilde{t}_1$. The sensitivity of the upper end of the p_T^H spectrum to the contribution of $\tilde{t}_1$, has already been discussed in some detail [61, 107]. The change of the shape of the p_T^H spectrum with the $\tilde{t}_1$ mass is estimated for MSSM benchmarks where the masses of all of the SUSY particles are set above 2 TeV, except for the scalar top and scalar bottom (sbottom) quarks. The sbottom gives only a small contribution to the cross section though. We vary $m_{\tilde{t}_1}$ from 500 GeV, close to current limits from direct searches at the LHC [108, 109], up to 1.5 TeV. The corresponding MSSM parameters are calculated with SoftSusy 4.1.7 [110], and the most relevant to our study are summarised in table 1. The p_T^H spectrum for the MSSM-like benchmarks is computed using SusHi 1.7.0 [111] interfaced with the output of SoftSusy, but setting the mass of the lightest Higgs boson to 125 GeV.[6]

The matched Wilson coefficient c_g can be expressed in terms of the MSSM masses and couplings as:

$$c_g = \frac{1}{96}\left(\frac{m_t^2}{m_{\tilde{t}_1}^2} g_{\tilde{t}_1} + \frac{m_t^2}{m_{\tilde{t}_2}^2} g_{\tilde{t}_2} + \frac{m_b^2}{m_{\tilde{b}_1}^2} g_{\tilde{b}_1} + \frac{m_b^2}{m_{\tilde{b}_2}^2} g_{\tilde{b}_2}\right), \tag{4.3}$$

where $g_{\tilde{t}}$ and $g_{\tilde{b}}$ are the Higgs couplings to the stop and sbottom quarks in the conventions of SusHi, while $c_{tg} = 0$, since the MSSM does not generate c_{tg} terms at leading order. Given the difference in the top and bottom quark masses, the value of c_g for our benchmark points is dominated by the stop contribution. The value of the coefficient c_t is about 0.998 for these scenarios, so that we can limit ourselves to consider the effects of c_g. Since $c_{tg} = 0$, the Wilson coefficients c_g, c_t do not run at LL-level.

The MSSM-like p_T^H spectra for different values of $m_{\tilde{t}_1}$ normalized to the SM predictions are compared in figure 5 to the corresponding SMEFT spectra for the c_g values obtained

[6] We note that, strictly speaking, the scenarios we are considering cannot be regarded as true MSSM benchmarks, since the ensuing mass of the SM-like Higgs boson would be below 125 GeV. However, here we are not interested in testing the MSSM, but in studying the validity of the EFT approach as a function of the masses of the BSM particles.

JHEP11(2021)173

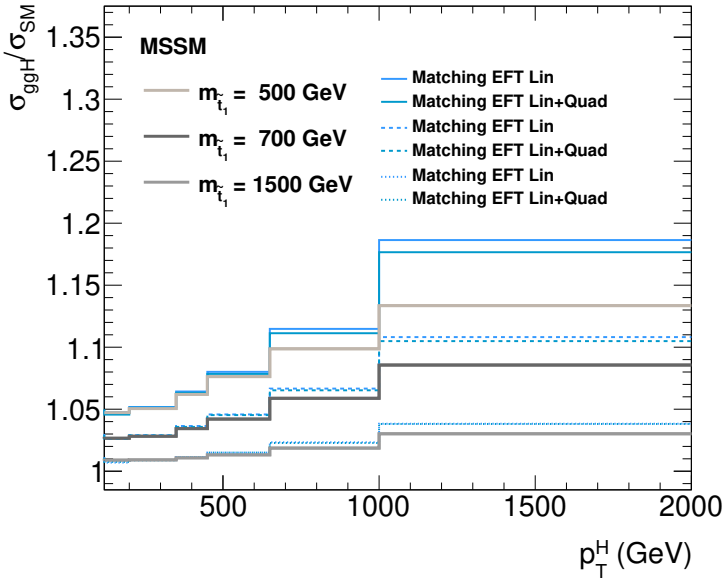

Figure 5. p_T^H spectra normalised to the SM prediction for the three MSSM-like benchmark points with varying $\tilde{t}_1$ masses. The SMEFT spectra for the matched Wilson coefficients and only linear and linear plus quadratic terms for the $m_{\tilde{t}}$=500 GeV and 1500 GeV benchmarks are also shown.

from the matching relation of eq. (4.3). Comparing figure 3 and figure 5 we see that the ratios R_i for the MSSM-like benchmarks are much closer to unity than those observed for the heavy top partner model. This is due to the fact that the MSSM particles decouple in the high-mass limit.

Fits to these spectra are performed over a p_T^H interval starting from 200 GeV up to an upper limit ranging from 450 GeV to 2 TeV. The c_g values extracted from the SMEFT fits are shown in figure 6 as a function of the upper limit of the fits. Similarly to what has been observed for the heavy top partner model in the previous section, the fitted c_g values are consistent with the matched values as long as the scalar top mass is significantly larger than the upper limit of the p_T^H range used in the fit. When transverse-momentum values above the stop mass are used in the fit ($p_T^H \gtrsim m_{\tilde{t}_1}$), the fitted values of c_g drop below the matched value of the model. It is interesting to observe how these trends indicate a sensitivity to New Physics from SMEFT fits beyond values of light stop masses already excluded by LHC direct searches [108, 109].

When comparing the results of SMEFT fits with linear and linear plus quadratic terms in figure 6 we observe a similar dependence of the fitted c_g values on the fit range in the linear SMEFT expansion as for the heavy top partner model. In the present case this dependence is milder because of the smaller values of c_g. On the other hand, the central fit values obtained with the linear SMEFT are slightly closer to the matched values. This might appear in contradiction with the fact that in figure 5 the linear plus quadratic curves are always closer to the actual MSSM-like spectra. However, in the fits performed for the MSSM-like scenarios the spectrum normalisation is kept as a free parameter, which changes this picture. The relatively large uncertainties associated to the fitted c_g values are a direct

JHEP11(2021)173

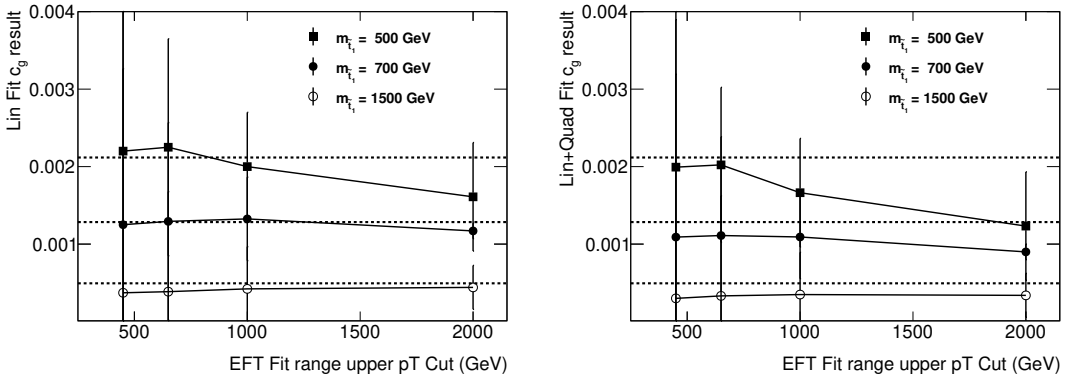

Figure 6. Wilson-coefficient c_g values obtained with only linear (left) and with linear plus quadratic terms (right) to p_T^H spectra produced from MSSM-like benchmark scenarios with different $m_{\tilde{t}_1}$ values as a function of the upper end of the p_T^H fit range. The dashed lines show the c_g values of the SMEFT matching to the MSSM-like benchmark scenarios.

consequence of the decoupling nature of the MSSM-like scenario under consideration and the small relative corrections with respect to the SM. Therefore, both linear and linear plus quadratic SMEFT fits are compatible with the c_g values obtained from the matching calculation within the range of applicability of the SMEFT, i.e. $p_T^H \lesssim m_{\tilde{t}_1}$. This is a consequence of the decoupling behaviour of the stops and sbottoms as BSM particles at the dimension-6 level so that the linear expansion provides a reliable approximation for the differential cross section in this case.

5 Results

This section presents the results of single- and multi-parameter SMEFT fits. The sensitivity of the LHC experiments to constrain the Wilson coefficients is studied by assuming a SM spectrum where the R_i ratios in all bins are equal to unity. The uncertainties correspond to those published by the experiments for the LHC Run 2 statistics and their extrapolations to the end of the HL-LHC programme at 3000 fb^{-1} assuming a combination of ATLAS and CMS data. The fits are performed either by using directly the R_i values from our scans and for the reference spectrum, thus being sensitive to both the spectrum shape and the Higgs signal yields normalised to the SM predictions, or by relying on the shape of the spectrum only, in which case only the relative change of the R_i values as a function of p_T^H are used in the fit. The sensitivity to constrain the Wilson coefficients of the two approaches is compared. The interplay of the ggF and $t\bar{t}H$ production modes in the SMEFT fits is studied for the case of a SM-like spectrum and SMEFT benchmarks. The results presented in section 5.2 include only the contribution of the ggF process, while those in section 5.3 also include $t\bar{t}H$ production. Finally, in section 5.4 the results reported by ATLAS and CMS are analysed in simultaneous fits to extract contours of the Wilson coefficients compatible with the current LHC data.

As mentioned above, constraints on the Wilson coefficients can also be obtained from the analysis of other processes. It is clear that constraints on c_t and c_g can be obtained

JHEP11(2021)173

from inclusive cross section measurements in the ggF and $t\bar{t}H$ channels. However, since there are blind directions in the c_t–c_g space, in the rest of the paper we will focus on high-p_T Higgs production in our analysis. On the other hand, the study of $t\bar{t}$ and single top differential cross sections is sensitive to c_{tg} [92, 112]. The CMS collaboration has reported bounds on the chromomagnetic dipole operator from the $t\bar{t}$ differential cross section in the azimuthal angle between the two leptons in di-leptonic events [113]. Other constraints have been obtained in ref. [114] by using top quark production with additional leptons. In the following we compare our results with the constraint on c_{tg} coming from the global analysis in the top sector recently reported in ref. [71], converted through eq. (2.6) to our conventions.

5.1 Experimental results for boosted Higgs production

The ATLAS and CMS experiments have performed several analyses of Higgs production at high p_T^H. The CMS collaboration has conducted a search for Higgs bosons produced with $p_T > 450\,\text{GeV}$ decaying to a $b\bar{b}$ pair based on the Run 2 data sample corresponding to an integrated luminosity of $137\,\text{fb}^{-1}$ [35]. The search obtains an observed signal strength $\mu_H = 3.7 \pm 1.6$ and reports an unfolded differential cross section in p_T^H bins for ggF production computed by assuming the other production modes at SM rates.

The ATLAS collaboration has reported preliminary results in a similar study for boosted Higgs production (inclusive over all production modes) in the $b\bar{b}$ final state on an integrated luminosity of $136\,\text{fb}^{-1}$ [37]. The study reports a signal strengths of $\mu_H = 0.7 \pm 3.3$ and $\mu_H = 26 \pm 31$ in the fiducial regions defined by $p_T^H \geq 450\,\text{GeV}$ and $p_T^H \geq 1\,\text{TeV}$, respectively, as well as unfolded inclusive signal strengths and differential cross sections in different p_T^H bins.

ATLAS has also obtained results for the boosted VH production process, again in the $H \to b\bar{b}$ decay channel, in the kinematic regions of $250 < p_T^V < 400\,\text{GeV}$ and $p_T^V > 400\,\text{GeV}$, where p_T^V is the transverse momentum of the W or Z boson emitted with the Higgs boson [115]. Finally, both collaborations have reconstructed the p_T^H spectrum using the $H \to \gamma\gamma$ and $H \to ZZ \to 4\ell$ decay channels [116, 117].

These studies give a significant corpus of results that can be used to derive experimental relative uncertainties in the measurements of the Higgs yields in p_T^H bins. The p_T^H binning used by the experiments for inclusive boosted Higgs production is [300-450], [450-650], $\geq 650\,\text{GeV}$ for CMS and [450-650], [650-1000], $\geq 1000\,\text{GeV}$ for ATLAS. ATLAS and CMS have also provided estimates for the evolution of these uncertainties with $3\,\text{ab}^{-1}$ of integrated luminosity at the HL-LHC [39, 118].

Our study is based on the latest results reported by ATLAS and CMS. At high p_T^H we use the results of the boosted $H \to b\bar{b}$ analyses, while for p_T^H values below those reported in the boosted analyses data are taken from the $H \to \gamma\gamma$ and $H \to ZZ \to 4\ell$ analyses.

5.2 Sensitivity of the ggF p_T^H spectrum to SMEFT parameters

In the following the sensitivity to constrain the Wilson coefficients from SMEFT fits for the ggF process to the p_T^H spectrum is studied by determining the regions in the SMEFT parameter space compatible with a SM-like spectrum, i.e. assuming R_i ratios equal to

JHEP11(2021)173

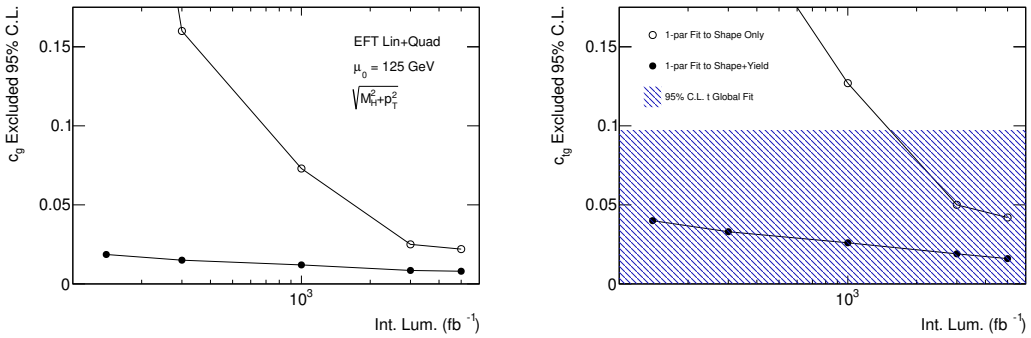

Figure 7. Values of the c_g (left) and c_{tg} (right) coefficients excluded at 95% C.L. as a function of the integrated luminosity $\int \mathcal{L}$ for single-parameter fits. The open points refer to fits to the spectrum shape only and the filled point to fits including also the Higgs signal yield normalised to the SM. The shaded horizontal strip in the right plot indicates the 95% C.L. interval for c_{tg} from the current top quark fit of ref. [71] translated to our definition of $c_{tg}(\mu_0)$.

unity in all p_T^H bins. When presenting results corresponding to an integrated luminosity of $140\,\text{fb}^{-1}$, the bound on c_{tg} reported in ref. [71] is shown as a blue-shaded band after translation to the conventions adopted in this paper. The translation of c_{tg} includes the conversion and running according to eq. (2.6) and eq. (2.4), respectively, assuming that ref. [71] uses an input value of $\mu_0 = m_t$.

First, we study the sensitivity to the c_g and c_{tg} coefficients as a function of the integrated luminosity $\int \mathcal{L}$ using the relative uncertainty on the determination of the Higgs p_T spectrum for $140\,\text{fb}^{-1}$ and $3000\,\text{fb}^{-1}$ and scaling it as $1/\sqrt{\int \mathcal{L}}$ for other values. This assumption is justified since the accuracy on the Higgs rate at high p_T^H is dominated by the statistical uncertainty. Figure 7 shows the values of c_g and c_{tg} that can be excluded at 95% C.L. in a single-parameter fit as a function of $\int \mathcal{L}$ by using either the spectrum shape only or also the signal yields in the fit, i.e. assuming $c_t(M_H) = 1.0$. We see that the constraint from such one-parameter fit on c_{tg} is already competitive with the constraint coming from top data [71]. These results demonstrate the significant improvement in accuracy achieved by adding the signal yield information, in particular when the available statistics is limited. The inclusion of LHC Run 3 data is expected to provide us with a significant improvement of the strength of the constraints obtained from the study of boosted Higgs production.

We continue with simultaneous fits of c_g and c_{tg} in figures 8–12. The regions of the SMEFT parameter space compatible with a SM-like spectrum are determined for different scenarios and assumptions in the multi-parameter fits. Similar to what was done before, the sensitivity of the fits obtained by using only the spectrum shape and also including the signal yields are compared. We have verified that, for values consistent with the current constraints obtained by ATLAS [119] and CMS [120] on the Higgs coupling modifier to top quarks, κ_t, in the κ-framework [121], the c_t coefficient does not induce significant modifications to the p_T^H spectrum shape and its contribution can be absorbed in a c_t^2 rescaling of the signal yield.

JHEP11(2021)173

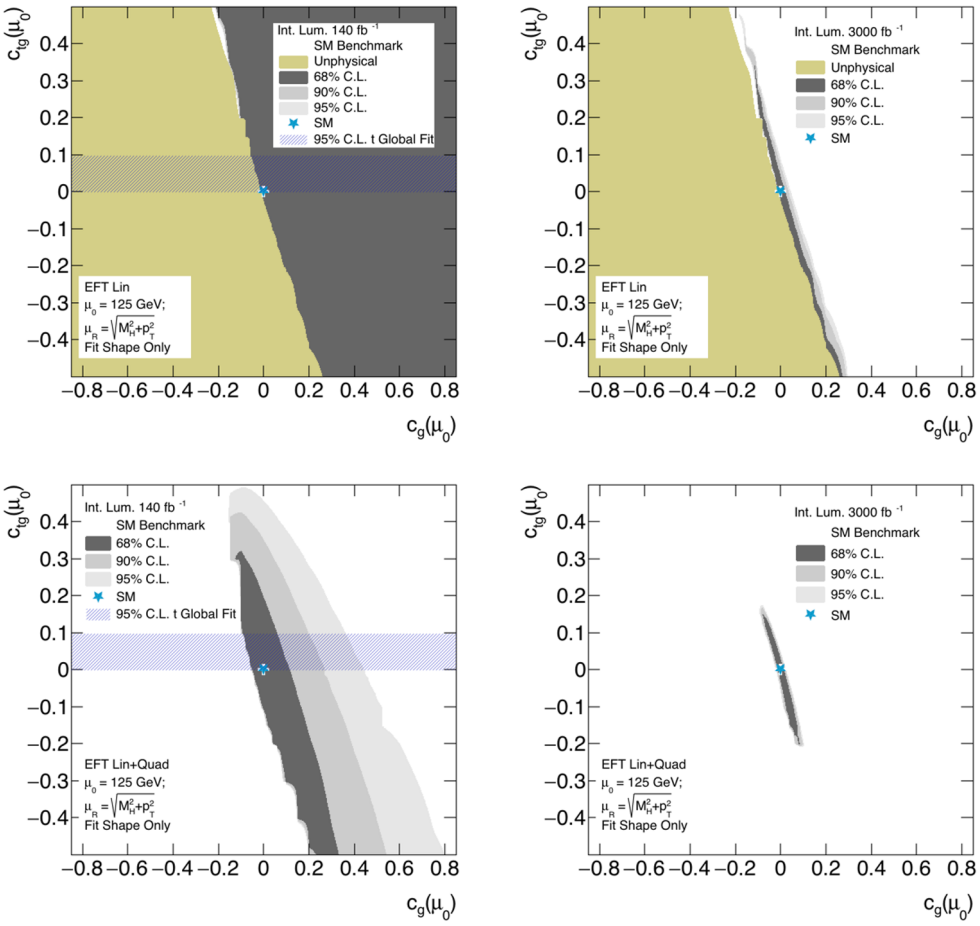

Figure 8. Constraints on the c_g and c_{tg} coefficients at 68% (dark grey), 90% (mid grey) and 95% (light grey) C.L. obtained from the fit to the spectrum shape on $200 < p_T^H < 2000\,\text{GeV}$ with $140\,\text{fb}^{-1}$ (left panels) and $3000\,\text{fb}^{-1}$ (right panels) for the linear (top panels) and with the addition of the quadratic terms (bottom panels). These constraints are obtained by including a free normalisation term in the fit and are therefore only sensitive to the spectrum shape. The SM value is indicated by the blue star and the best fit value by the white marker. The shaded horizontal strip indicates the 95% C.L. interval for c_{tg} from the top quark fit of ref. [71] translated to our definition of $c_{tg}(\mu_0)$. The region shown in colour and labelled "unphysical" in the fits with only SMEFT linear terms indicates the parameter space leading to negative unphysical values of cross section in the p_T^H spectrum for a linear SMEFT approximation at dimension 6.

Furthermore, we compare the results obtained with a linear SMEFT expansion and an expansion including also quadratic terms in the Wilson coefficients. As discussed in section 2 the default scale choice for our analysis is a dynamical factorization and renormalization scale $\mu_R = \mu_F = \sqrt{M_H^2 + p_T^2}$. As for the input scale μ_0 for the Wilson coefficients, we adopt the natural choice $\mu_0 = 125\,\text{GeV}$, but, for comparison, we also show results for $\mu_0 = 1\,\text{TeV}$.

The experimental uncertainties are taken from the ATLAS and CMS Run 2 public analyses ($140\,\text{fb}^{-1}$) and those expected for the HL-LHC with twenty times larger data sets

JHEP11(2021)173

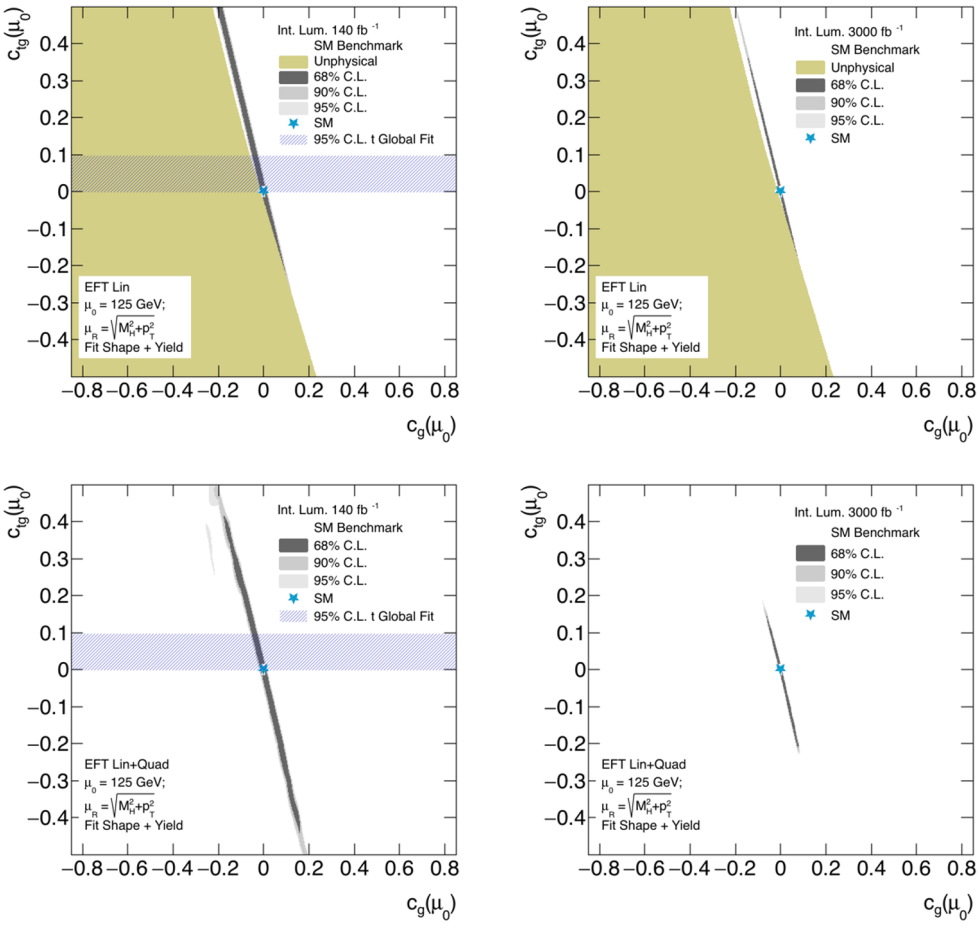

Figure 9. Constraints on the c_g and c_{tg} coefficients at 68% (dark grey), 90% (mid grey) and 95% (light grey) C.L. obtained from the fit to the spectrum shape and Higgs signal rate on $200 < p_T^H < 2000\,\text{GeV}$ with $140\,\text{fb}^{-1}$ (left panels) and $3000\,\text{fb}^{-1}$ (right panels) for the linear (top panels) and with the addition of the quadratic terms (bottom panels). The SM value is indicated by the blue star and the best fit value by the white marker. The shaded horizontal strip indicates the 95% C.L. interval for c_{tg} from the top quark fit of ref. [71] translated to our definition of $c_{tg}(\mu_0)$. The region shown in colour and labelled "unphysical" in the fits with only SMEFT linear terms indicates the parameter space leading to negative unphysical values of cross section in the p_T^H spectrum for a linear SMEFT approximation at dimension 6.

$(3000\,\text{fb}^{-1})$. The relative uncertainties for the signal strengths in each p_T^H bin are computed by combining the total uncertainties for ATLAS and CMS. We also assume a theoretical uncertainty of 12% in all p_T^H bins.

Figure 8 compares the sensitivity of the fits in the c_{tg}–c_g plane for $140\,\text{fb}^{-1}$ and $3000\,\text{fb}^{-1}$ of integrated luminosity (left vs. right plot) as well as the difference between only linear against also quadratic terms in the SMEFT expansion (top vs. bottom plots). While in figure 8 only the shape information of the spectrum is used, the contours in figure 9 are obtained from a fit that includes also the Higgs signal yields normalised to the SM. The results from the fits to the spectrum shapes and Higgs signal rates are not significantly

JHEP11(2021)173

modified if the assumption of $c_t(M_H) = 1.0$ is relaxed by imposing instead a constraint on $c_t(M_H)$ corresponding to the κ_t bounds reported by ATLAS [119] and CMS [120].

The use of SMEFT linear terms only can result in negative values of the Higgs cross section for some p_T^H values in our fit range over a relatively large region of the c_g, c_{tg} Wilson coefficients, which are marked as "unphysical" in the respective figures. This is not unexpected and can be explained as an effect of the interference term between dimension-4 and dimension-6 operators, which can be negative, in absence of the squared contributions of the dimension-6 operators.

When comparing the top and bottom plots in figure 8 and figure 9, we observe that the inclusion of the SMEFT quadratic terms results in tighter constraints on the Wilson coefficients. Whether quadratic terms should or should not be included in dimension-6 SMEFT fits is still an open question: including quadratic terms corresponds to promote the SMEFT expansion from the level of the Lagrangian to the amplitude level. As we have seen in section 4.1 and section 4.2, the issue is also related to the decoupling behaviour of the underlying UV model.

The effects from including quadratic terms are particularly significant in figure 8 where the fits include a free normalisation parameter and are therefore only sensitive to the spectrum shape and not to the Higgs signal yields normalised to the SM. Comparing the left and right panels in figure 8 and figure 9, it is also clear that with the statistical accuracy at $3000\,\text{fb}^{-1}$ the constraints will substantially improve and also become significantly more stable with respect to the various choices that can be made in the fits. Disregarding the case of the shape-only fit with linear terms (upper left plot in figure 8) for which the sensitivity obtained at $140\,\text{fb}^{-1}$ is still limited, we observe a significant anti-correlation between the c_g and c_{tg} coefficients defining elongated contours where they are compatible with a SM-like spectrum.

Up to now all our results have been obtained by using a dynamical renormalisation and factorisation scale $\mu_R = \mu_F = \sqrt{M_H^2 + p_T^2}$. In the case in which all the scales are fixed to $\mu_F = \mu_R = \mu_0 = M_H$ the constraints obtained for a SM-like spectrum would be tighter by $\simeq$10%. This, however, is originating from an ill-defined treatment of logarithmic contributions at higher orders and should not be viewed as an improvement.

Finally, we consider the case in which the reference scale μ_0 is chosen as $\mu_0 = 1\,\text{TeV}$, instead of $\mu_0 = 125\,\text{GeV}$, still using a dynamical scale $\mu_R = \mu_F = \sqrt{M_H^2 + p_T^2}$. The corresponding results are shown in figure 10. Comparing with figure 9, we observe that the correlation between c_{tg} and c_g is reversed. This is due to the fact that the RG equation for c_g has a large term driven by c_{tg}, see eq. (2.4). However, the two results are fully compatible and can be directly obtained from each other by translating each point in the parameter space for one μ_0 scale choice to the other through the RG evolution of the Wilson coefficients. The last two results underline the importance of including the RG running of the Wilson coefficients and properly specifying the input scale of the fit.

5.3 Interplay of ggF and $t\bar{t}H$ production in the p_T^H SMEFT fits

The results presented so far are based on the study of the SMEFT effects in Higgs production through gluon fusion. Although these effects are dominant, as discussed in section 3.1,

JHEP11(2021)173

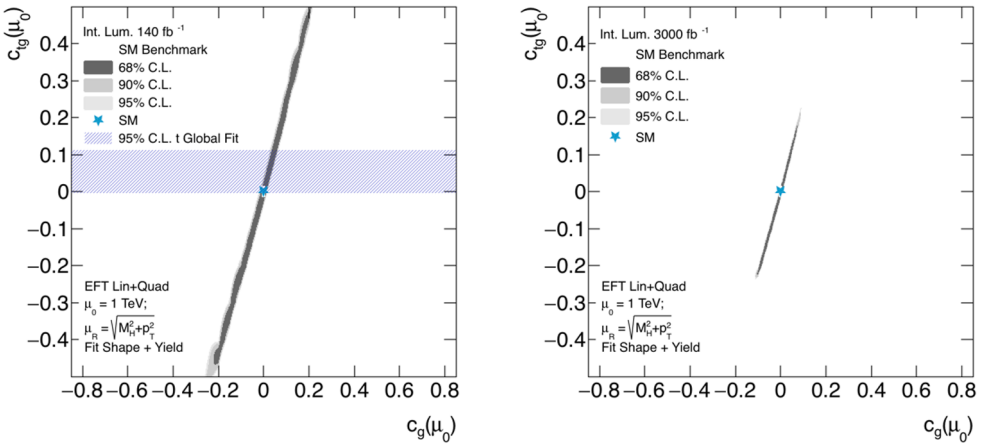

Figure 10. Constraints on the c_g and c_{tg} coefficients at 68% (dark grey), 90% (mid grey) and 95% (light grey) C.L. obtained from the fit to the spectrum shape and Higgs signal rate on $200 < p_T^H < 2000\,\text{GeV}$ with $140\,\text{fb}^{-1}$ (left panel) and $3000\,\text{fb}^{-1}$ (right panel) for $\mu_0 = 1\,\text{TeV}$. The SM value is indicated by the blue star and the best fit value by the white marker. The shaded horizontal strip indicates the 95% C.L. interval for c_{tg} from the top quark fit of ref. [71] translated to our definition of $c_{tg}(\mu_0)$.

in general the experimental analyses select a mixture of boosted Higgs events from all production modes. In particular, the ggF and $t\bar{t}H$ production processes are sensitive to the same SMEFT operators. Therefore, it is interesting to study the effect of including both ggF and $t\bar{t}H$ contributions in the SMEFT fits of the Wilson coefficients. Again we consider a SM-like spectrum where the R_i ratios are equal to unity in all p_T^H bins with the relative uncertainties taken from the experimental measurements and projections. Additionally, benchmark scenarios with non-zero c_g and/or c_{tg} values are fitted, assuming the same relative uncertainties. As discussed in section 3, the simultaneous fit of the ggF and $t\bar{t}H$ SMEFT spectra is based on the sum of the R_i ratios for each process weighted by the respective fraction, f, of signal events in the sample. For the VH and VBF processes, whose spectra are not sensitive to the $\mathcal{O}_1$, $\mathcal{O}_2$ and $\mathcal{O}_3$ SMEFT operators, a SM-like contribution is assumed.

First, the regions in the c_g–c_{tg} parameter space compatible with a SM-like spectrum are determined assuming $f_{ggF} = 0.50$ and $f_{t\bar{t}H} = 0.15$, consistent with the fractions of signal events obtained by the experimental analyses. The results are shown in figure 11 for $140\,\text{fb}^{-1}$ and $3000\,\text{fb}^{-1}$, including linear and quadratic terms as well as p_T^H shape and signal yield information in the fit for $\mu_0 = 125\,\text{GeV}$. Comparing the results in figure 11 to those in the corresponding two lower plots of figure 9, the additional correlation between the two Wilson coefficients, induced by the not negligible sensitivity offered by the $t\bar{t}H$ process to c_{tg}, is evident, in particular when c_g is small. For example, in the case of $140\,\text{fb}^{-1}$, we see that the extreme values of the allowed region in the ggF-only fit ($c_{tg} \sim \pm 0.4$, $c_g \sim \pm 0.2$) are now completely excluded. Indeed, the strong (anti-)correlation of c_g and c_{tg} resulting from the ggF-only fit is largely reduced yielding a more circular shape in the c_g–c_{tg} plane.

JHEP11(2021)173

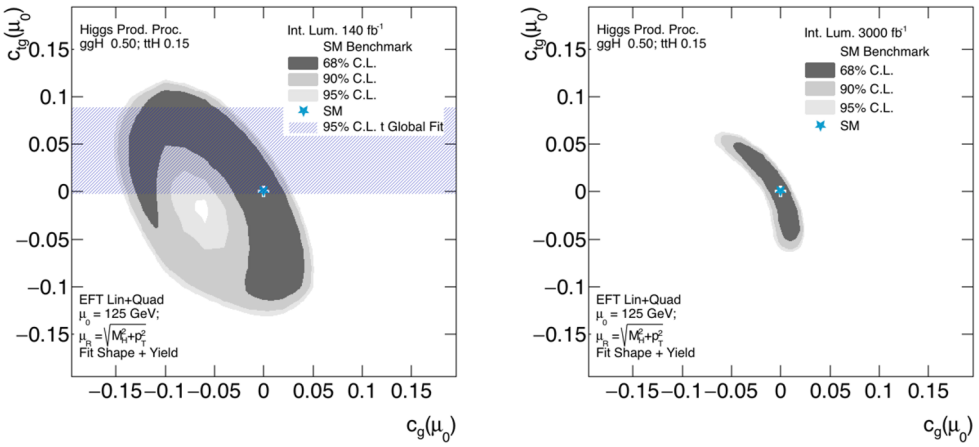

Figure 11. Constraints on the c_g and c_{tg} coefficients at 68% (dark grey), 90% (mid grey) and 95% (light grey) C.L. obtained from the fit including ggF and $t\bar{t}H$ SMEFT contributions to the SM-like spectrum shape and Higgs signal rate on $200 < p_T^H < 2000\,\text{GeV}$ with $140\,\text{fb}^{-1}$ (left panel) and $3000\,\text{fb}^{-1}$ (right panel). The SM value is indicated by the blue star and the best fit value by the white marker. The shaded horizontal strip indicates the 95% C.L. interval for c_{tg} from the top quark fit of ref. [71] translated to our definition of $c_{tg}(\mu_0)$. Notice also the reduced range compared to figure 9.

We continue by considering benchmark spectra generated by combining SM-normalised SMEFT distributions for the ggF and $t\bar{t}H$ processes corresponding to a set of Wilson coefficients. The values of c_g, c_{tg} compatible with these benchmark spectra are determined by fitting them either with templates for the consistently combined ggF and $t\bar{t}H$ predictions or by using only ggF predictions, while assuming all the other Higgs production processes to be SM-like. Figure 12 shows the constraints obtained for a benchmark with $c_g(\mu_0) = 0$ and $c_{tg}(\mu_0) = 0.10$ fitted with the same ggF (0.50) and $t\bar{t}H$ (0.15) SMEFT contributions used to generate the benchmark spectrum. This point in the parameter space is chosen at c_g=0 and at the upper bound on c_{tg} obtained by the fit to top-quark data of ref. [71] where the $t\bar{t}H$ effects are largest. The ggF plus $t\bar{t}H$ fit correctly recovers the input benchmark values. Instead, if this spectrum is fitted assuming the $t\bar{t}H$ contribution to be SM-like, the fit yields $c_g(\mu_0) = -0.04 \pm 0.07$ and $c_{tg}(\mu_0) = 0.17 \pm 0.33$ for $140\,\text{fb}^{-1}$ and $c_g(\mu_0) = -0.04 \pm 0.01$ and $c_{tg} = 0.19 \pm 0.04$ for $3000\,\text{fb}^{-1}$ of integrated luminosity. Similarly, a benchmark $c_g(\mu_0) = 0.02$ and $c_{tg}(\mu_0) = 0.08$ gives fit values of $c_g(\mu_0) = -0.02 \pm 0.01$ and $c_{tg}(\mu_0) = 0.14 \pm 0.03$ for $3000\,\text{fb}^{-1}$ of integrated luminosity. This indicates that the assumption of a SM-like $t\bar{t}H$ contribution in the SMEFT fit gives results that are still statistically compatible with the benchmark true parameters at the current level of accuracy, but these would become significantly biased with the uncertainties anticipated for the HL-LHC. We conclude that a global fit including the ggF and $t\bar{t}H$ SMEFT contributions weighted by the corresponding fractions of signal events selected by the experimental analysis will be required for HL-LHC analyses.

JHEP11(2021)173

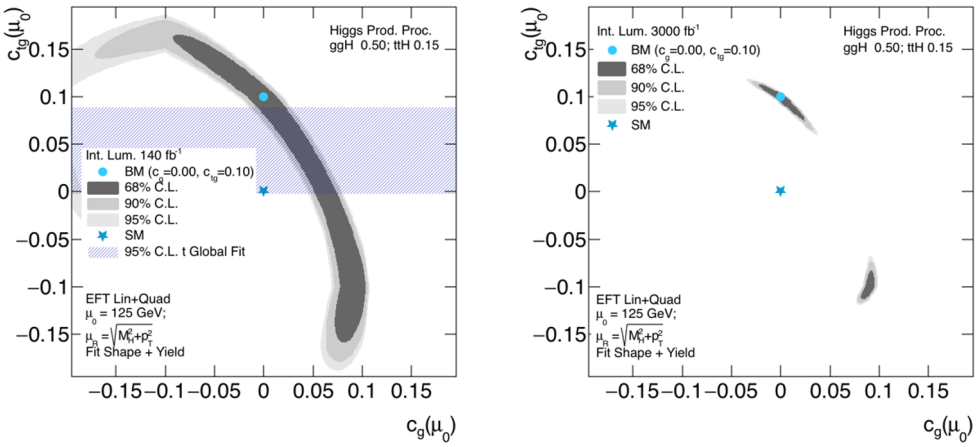

Figure 12. Constraints on the c_g and c_{tg} coefficients at 68% (dark grey), 90% (mid grey) and 95% (light grey) C.L. obtained from the fit including ggF (0.50) and $t\bar{t}H$ (0.15) SMEFT contributions to the spectrum shape and Higgs signal rate on $200 < p_T^H < 2000\,\text{GeV}$ with $140\,\text{fb}^{-1}$ (left panel) and $3000\,\text{fb}^{-1}$ (right panel) for a benchmark point with $c_g(\mu_0) = 0$ and $c_{tg}(\mu_0) = 0.1$. The benchmark value is indicated by the dark blue circle. The shaded horizontal strip indicates the 95% C.L. interval for c_{tg} from the top quark fit of ref. [71] translated to our definition of $c_{tg}(\mu_0)$.

5.4 Fit of the ggF spectrum to experimental results

The ATLAS and CMS collaborations have already published constraints on the SMEFT parameters obtained by fits to their p_T^H results [122, 123]. However, the early ATLAS analysis for ggF production at high p_T^H of ref. [123] only used the $H \to \gamma\gamma$ results for $p_T^H \geq 450\,\text{GeV}$ in their fits, while the CMS SMEFT result of ref. [122] was based on the preliminary boosted $H \to b\bar{b}$ analysis performed with only $35\,\text{fb}^{-1}$ of integrated luminosity. Here we provide a first assessment of the values of the Wilson coefficients compatible with the current LHC results from both experiments, while consistently accounting for their RG evolution. Since no combination is available of the p_T^H spectra measured by ATLAS and CMS, we obtain constraints from the data of the two experiments by performing a simultaneous SMEFT fit to the two independent sets of signal strenghts in the p_T^H bins reported by the two experiments. The uncertainties on these measurements are largely dominated by the statistical contributions, correlations between the two results are expected to be small at the current level of accuracy and are neglected here.

The ATLAS preliminary analysis is inclusive, i.e. the signal strengths are not separated by Higgs production modes. The CMS analysis reports results for ggF signal strengths assuming the other production modes to be SM-like. Therefore, we consider only the ggF SMEFT contribution in our study, and the ATLAS signal strength values and related uncertainties are rescaled by the inverse of the relative ggF contribution reported by ATLAS in each p_T^H bin.

The fit is performed by keeping the c_g and c_{tg} parameters free. Given the limited accuracy of the current experimental results only the fits using both the spectrum shape and the signal event rate as well as including both linear and quadratic SMEFT terms offer

JHEP11(2021)173

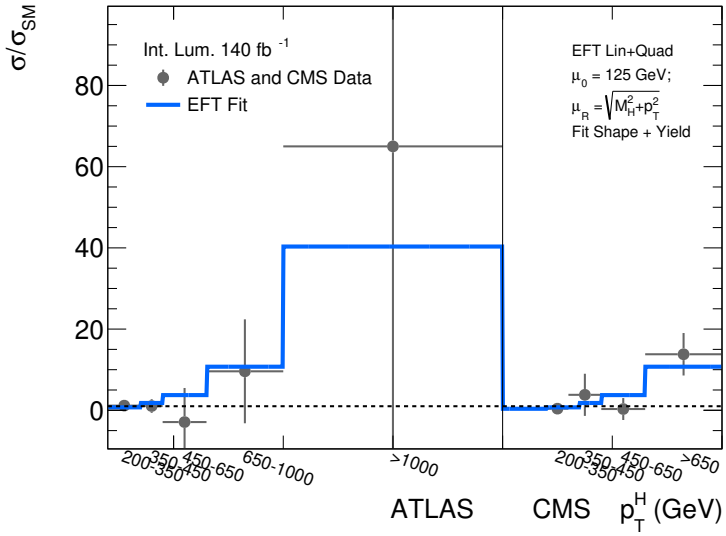

Figure 13. Result of a simultaneous fit to the spectrum shape and Higgs signal rate of ATLAS (left) and CMS (right) using the SMEFT expansion with linear and quadratic terms at $\mu_0 = 125\,\text{GeV}$. The points with error bars show the data and the continuous line the best fit corresponding to $c_g(M_H) = -0.08$ and $c_{tg}(M_H) = -0.13$.

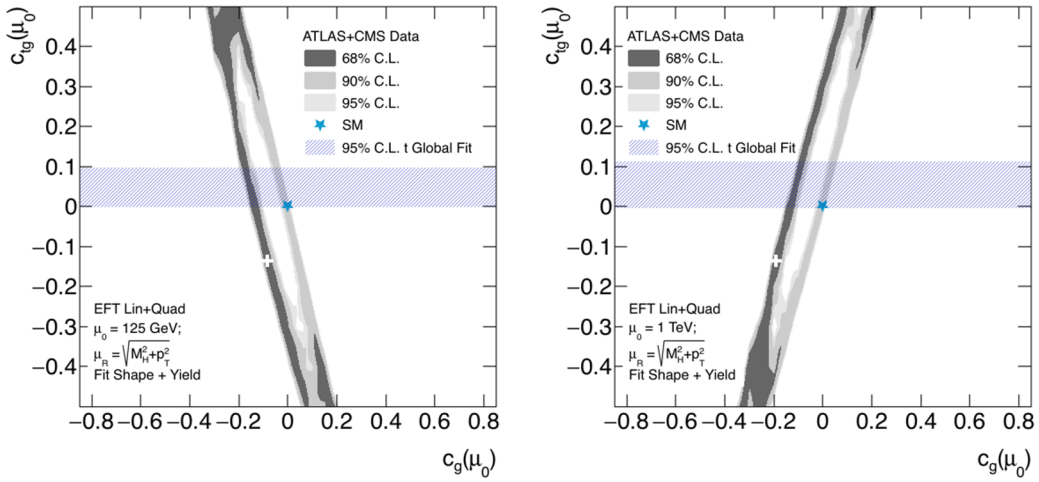

Figure 14. Constraints on the c_g and c_{tg} coefficients at 68% (dark grey), 90% (mid grey) and 95% (light grey) C.L. obtained from the simultaneous fit to ATLAS and CMS data for $\mu_0 = 125\,\text{GeV}$ (left panel) and $\mu_0 = 1\,\text{TeV}$ (right panel). The SM value is indicated by the blue star and the best fit value by the white marker. The shaded horizontal strip indicates the 95% C.L. interval for c_{tg} from the top quark fit of ref. [71] translated to our definition of $c_{tg}(\mu_0)$.

some sensitivity to the Wilson coefficients, see section 5.2. Therefore our fit does not include the normalisation parameter, i.e. assuming $c_t(M_H) = 1.0$, and it uses linear and quadratic terms in the SMEFT expansion. The results of a simultaneous fit to the preliminary ATLAS and the CMS data is shown in figure 13 for the best fit values $c_g(M_H) = -0.08$ and $c_{tg}(M_H) = -0.13$. The corresponding contraints in the c_{tg}–c_g plane obtained for two choices of the RG input scale, $\mu_0 = 125\,\text{GeV}$ and $\mu_0 = 1\,\text{TeV}$, are summarised in figure 14 with data compatible with the SM at better than 90% C.L.

JHEP11(2021)173

The fit yields a contour in the parameter space compatible with the data within 90% C.L that can be described as a very elongated ellipse with an elliptic hole in the middle. This essentially leads to two disjoint sets of solutions along almost parallel lines. The SM point lies close to the edge of one of these lines, while the best fit value belongs to the other parallel branch. These features are fully preserved when changing the input scale μ_0 from 125 GeV to 1 TeV. However, as observed in figure 10, the use of the reference scale $\mu_0 = 1$ TeV leads to a striking modification of the correlation in the c_{tg}–c_g plane. As discussed in section 5.2, this effect is due to the large impact of the c_{tg} term in the RG equation of the c_g coefficient, see eq. (2.4). The two results can be consistently translated into each other by using the RG evolution of the operators.

6 Conclusions

In this paper we have considered Higgs boson production at large transverse momentum, a new stage in the study of the Higgs profile at the LHC. The effects of the three leading dimension-6 operators in the gluon-fusion and $t\bar{t}H$ production processes have been studied in the Standard Model Effective Field Theory. They include a point-like Higgs-gluon coupling, the chromomagnetic dipole operator of the top quark and a reweighting of the top-quark Yukawa coupling. The corresponding Wilson coefficients c_g, c_{tg} and c_t have been defined as scale dependent quantities obeying renormalization group equations coupled among the three operators.

The central goal of our study has been to place bounds on the Wilson coefficients of the dimension-6 operators from current LHC data and to assess the sensitivity that can be reached throughout the LHC programme. This has been achieved through multi-parameter χ^2 fits of the deviations of the Higgs production cross section computed in SMEFT in bins of Higgs p_T combined with the available state-of-the-art SM predictions for the ggF and $t\bar{t}H$ channels, taking into account the experimental and theoretical uncertainties.

Although not yet critical at the current level of experimental accuracy, accounting for renormalisation group evolution of the SMEFT operators is crucial when it comes to precision bounds on the Wilson coefficients. Our analysis employs a dynamical renormalisation and factorisation scale, which is set to the transverse mass of the Higgs boson for the ggF production mode. To account for the correct momentum transfer in the SMEFT couplings the dynamical setting of the renormalization scale is used also for the Wilson coefficients. In the fits the Wilson coefficients are then extracted at an input scale μ_0 equal to the Higgs mass. We have shown that the use of a high scale $\mu_0 = 1$ TeV would lead to a completely different correlation between c_g and c_{tg} when performing multi-parameter fits in the c_{tg}–c_g plane. With an analysis spanning a wide range of Higgs transverse momenta, running effects are important. It is therefore advisable to present results including the running of the operators as this will become essential for HL-LHC analysis.

The validity of the SMEFT assumptions has been tested by performing fits to a model with a heavy-top partner and to MSSM-like scenarios with a light scalar top, varying the new particle masses and the p_T^H range used in the fits. The Wilson coefficients extracted from the fits agree with the values obtained by calculating the matching between the

JHEP11(2021)173

explicit model and the SMEFT as long as the upper end of the p_T^H range used in the fits is not significantly larger than the mass of the heavy particle in the model. We have also contrasted the results obtained with only linear or linear plus quadratic terms in the SMEFT expansion. In the case in which new physics does not decouple, as it happens in scenarios with a heavy top partner, SMEFT effects are large and a fit with linear and quadratic terms yields results that are closer to those obtained in the full model. Instead, when the new physics decouples, as in the case of the MSSM-like model with a light scalar top and heavy SUSY particles, the new physics effects are small and can be captured already through a fit including only linear terms in the SMEFT expansion.

The sensitivity to the c_g and c_{tg} Wilson coefficients has been studied for both the current accuracy and for future LHC accuracies of boosted Higgs production. The use of both the shape of the p_T^H spectrum and the signal yield provide stringent constraints on the Wilson coefficients, with a peculiar (anti-)correlation in the c_{tg}–c_g plane. The constraint on c_{tg} extracted from a single-parameter fit to a SM-like Higgs p_T^H spectrum appears to be competitive with the corresponding bound obtained from a multi-parameter fit in the global analysis of the top sector recently reported in ref. [71]. The constraints in the c_{tg}–c_g plane will become rather tight with the anticipated accuracy obtained with HL-LHC data.

In the range allowed by the current ATLAS and CMS constraints on the Higgs coupling modifier to top quarks, κ_t, the c_t Wilson coefficient does not induce significant modifications to the p_T^H spectrum shape. Moreover, it is clear that constraints on c_t will come from inclusive cross section measurements, especially from $t\bar{t}H$ production, while the Higgs transverse-momentum spectrum will then yield an accurate determination of the Wilson coefficients c_g and c_{tg}.

Most of our results have been obtained by focusing on the ggF production mode. However, we have also investigated the interplay between the ggF and $t\bar{t}H$ Higgs production, which are both sensitive to the same set of Wilson coefficients, assuming the other Higgs production modes to be SM-like. The SMEFT effects from $t\bar{t}H$ production are subdominant and its inclusion does not lead to substantial effects for current uncertainties, with the exception of the region at low c_g and large c_{tg} values where the effects from $t\bar{t}H$ production are largest. These effects are not yet observable in the current LHC analyses, but will need to be included as the experimental accuracy will improve. Moreover, we stress that with future uncertainties the combination of ggF and $t\bar{t}H$ in SMEFT fits will enable the reduce the correlation of c_g and c_{tg} and lead to stringent constraints on both of them simultaneously.

Finally, we have extracted constraints on the c_g and c_{tg} for ggF production from a simultaneous fit to the preliminary ATLAS and the CMS data and compared our results with those obtained in a global SMEFT analysis in the top sector. With the current data the ATLAS and CMS results are compatible with the SM at better than 90% C.L.

Acknowledgments

We are grateful to Andrea Sciandra for his contribution in the early stages of this work, to Eleni Vryonidou for useful correspondence and to Hannah Arnold and Pietro Slavich

JHEP11(2021)173

for comments on the manuscript. M.B. thanks the Galileo Galilei Institute for Theoretical Physics, Arcetri, Florence, for hospitality and support during part of the preparation of this study. The work of M.G. is supported in part by the Swiss National Foundation under contract 200020_188464.

A Running of the Wilson coefficients

In this appendix we describe the solution of the renormalization-group equations (RGEs) at the leading-log level. We have extracted the RGEs from ref. [64] and confirmed the leading-log part by the corresponding results of refs. [72–74]. In order to translate the notation of ref. [64] into our notation of eq. (2.3), we used the following relations,

$$\begin{aligned} C_1 &= -(c_t - 1)\frac{\sqrt{2}m_t}{v}\,\frac{\Lambda^2}{v^2}\,, \\ C_2 &= \frac{c_g}{8\pi^2}\,\frac{\Lambda^2}{v^2}\,, \\ C_3 &= c_{tg}\frac{m_t}{\sqrt{2}v}\,\frac{\Lambda^2}{v^2}\,, \end{aligned} \tag{A.1}$$

where $v = 1/\sqrt{\sqrt{2}G_F}$ denotes the vacuum expectation value of the Higgs field and m_t the top mass, while Λ represents the cut-off scale of the SMEFT framework. The parameters m_t and the Wilson coefficients c_t, c_g and c_{tg} evolve either due to strong interactions or due to the top-Yukawa coupling in our QCD analysis. The relevant RGEs for our work at the leading-log level are ($a_s = \alpha_s/\pi$),

$$\begin{aligned} \partial_t C_1 &= -a_s\, C_1 + 8\frac{m_t^2}{v^2}\, a_s\, C_3\,, \\ \partial_t C_2 &= \frac{m_t}{8\sqrt{2}\pi^2 v}\, C_3\,, \\ \partial_t C_3 &= \frac{a_s}{6}\, C_3\,, \end{aligned} \tag{A.2}$$

where $\partial_t = \partial/\partial t$, with $t = \log(Q^2/\mu^2)$ with Q being the scale of the physical process and μ the input scale of the RG-evolution. The corresponding RGEs for our parameters can be derived from eq. (A.2),[7]

$$\begin{aligned} \partial_t c_t &= -4\frac{m_t^2}{v^2}\, a_s\, c_{tg}\,, \\ \partial_t c_g &= \frac{m_t^2}{2v^2}\, c_{tg}\,, \\ \partial_t c_{tg} &= \frac{7a_s}{6}\, c_{tg}\,. \end{aligned} \tag{A.3}$$

[7] We note that consistent with the leading-logarithmic level we are neglecting additional contributions of higher order in a_s or m_t^2. Therefore higher-order c_g and c_{3G} terms are dropped in the RGE for c_{tg}, where c_{3G} is the dimension-six Wilson coefficient of the three-gluon operator GGG.

JHEP11(2021)173

The simplicity of these RGEs underlines the suitability of our conventions in eq. (2.3), i.e. the leading QCD evolution is factored out, leaving us with pure EFT effects on the scale dependence in eq. (A.3). If c_{tg} vanishes at the input scale μ, there is no scale dependence of our Wilson coefficients c_t, c_g, c_{tg} at LL-level. For the SM parameters, we use the 5-flavour scheme, i.e. all effects at the scale of the top mass and beyond are decoupled from the running in compatibility with the definition of the strong coupling α_s in the PDF fits,

$$\begin{aligned} \partial_t m_t &= -a_s\, m_t\,, \\ \partial_t a_s &= -\beta_0 a_s^2\,, \end{aligned} \tag{A.4}$$

with $\beta_0 = (33 - 2N_F)/12 = 23/12$ denoting the leading-order beta function coefficient of QCD. The second RGE for a_s can be used as usual to replace the integration measure t by an integration over a_s,

$$dt = -\frac{da_s}{\beta_0 a_s^2}\,. \tag{A.5}$$

This allows us to solve the RGEs for the running top mass and the Wilson coefficient C_3 immediately at LL level,

$$\begin{aligned} m_t(Q^2) &= m_t(\mu^2) \left(\frac{a_s(Q^2)}{a_s(\mu^2)}\right)^{\frac{1}{\beta_0}}\,, \\ C_3(Q^2) &= C_3(\mu^2) \left(\frac{a_s(Q^2)}{a_s(\mu^2)}\right)^{-\frac{1}{6\beta_0}}\,. \end{aligned} \tag{A.6}$$

The solution for C_3 corresponds to the following LL expression for c_{tg},

$$c_{tg}(Q^2) = c_{tg}(\mu^2) \left(\frac{a_s(Q^2)}{a_s(\mu^2)}\right)^{-\frac{7}{6\beta_0}}\,. \tag{A.7}$$

Using the solutions for m_t and c_{tg}, the RGEs for c_t and c_g can be solved,

$$\begin{aligned} c_t(Q^2) &= c_t(\mu^2) + \frac{24}{5}\,\frac{m_t^2(\mu^2)}{v^2}\, c_{tg}(\mu^2)\, \left\{\left(\frac{a_s(Q^2)}{a_s(\mu^2)}\right)^{\frac{5}{6\beta_0}} - 1\right\}\,, \\ c_g(Q^2) &= c_g(\mu^2) - \frac{3}{5-6\beta_0}\,\frac{m_t^2(\mu^2)}{v^2}\,\frac{c_{tg}(\mu^2)}{a_s(\mu^2)}\, \left\{\left(\frac{a_s(Q^2)}{a_s(\mu^2)}\right)^{\frac{5}{6\beta_0}-1} - 1\right\}\,. \end{aligned} \tag{A.8}$$

In order to cope with pure QCD effects beyond the LL level, we are adding the next-to-leading QCD part to the RGEs of a_s and c_g,

$$\begin{aligned} \partial_t a_s &= -\beta_0 a_s^2 - \beta_1 a_s^3\,, \\ \partial_t c_g &= \frac{m_t^2}{2v^2}\, c_{tg} - \beta_1 a_s^2 c_g\,, \end{aligned} \tag{A.9}$$

JHEP11(2021)173

where $\beta_1 = (153 - 19N_F)/24 = 29/12$ denotes the NLO coefficient of the QCD beta function. The final solution of the RG running for c_g can then be extended approximately as

$$c_g(Q^2) = \frac{\beta_0 + \beta_1 a_s(Q^2)}{\beta_0 + \beta_1 a_s(\mu^2)} \left\{ c_g(\mu^2) - \frac{3}{5 - 6\beta_0} \frac{m_t^2(\mu^2)}{v^2} \frac{c_{tg}(\mu^2)}{a_s(\mu^2)} \left[\left(\frac{a_s(Q^2)}{a_s(\mu^2)} \right)^{\frac{5}{6\beta_0} - 1} - 1 \right] \right\}, \tag{A.10}$$

where the error is of next-to-leading-logarithmic order for the top Yukawa-induced contributions, while the leading QCD part agrees with the known scale dependence of the trace-anomaly coefficient [124–129]. As seen from eq. (A.10), when c_{tg} vanishes only the pure QCD running of c_g remains.

References

[1] ATLAS collaboration, *Observation of a new particle in the search for the Standard Model Higgs boson with the ATLAS detector at the LHC*, *Phys. Lett. B* **716** (2012) 1 [arXiv:1207.7214] [INSPIRE].

[2] CMS collaboration, *Observation of a New Boson at a Mass of 125 GeV with the CMS Experiment at the LHC*, *Phys. Lett. B* **716** (2012) 30 [arXiv:1207.7235] [INSPIRE].

[3] T. Appelquist and J. Carazzone, *Infrared Singularities and Massive Fields*, *Phys. Rev. D* **11** (1975) 2856 [INSPIRE].

[4] C.J.C. Burges and H.J. Schnitzer, *Virtual Effects of Excited Quarks as Probes of a Possible New Hadronic Mass Scale*, *Nucl. Phys. B* **228** (1983) 464 [INSPIRE].

[5] C.N. Leung, S.T. Love and S. Rao, *Low-Energy Manifestations of a New Interaction Scale: Operator Analysis*, *Z. Phys. C* **31** (1986) 433 [INSPIRE].

[6] W. Buchmüller and D. Wyler, *Effective Lagrangian Analysis of New Interactions and Flavor Conservation*, *Nucl. Phys. B* **268** (1986) 621 [INSPIRE].

[7] B. Grzadkowski, M. Iskrzynski, M. Misiak and J. Rosiek, *Dimension-Six Terms in the Standard Model Lagrangian*, *JHEP* **10** (2010) 085 [arXiv:1008.4884] [INSPIRE].

[8] I. Brivio and M. Trott, *The Standard Model as an Effective Field Theory*, *Phys. Rept.* **793** (2019) 1 [arXiv:1706.08945] [INSPIRE].

[9] F. Feruglio, *The Chiral approach to the electroweak interactions*, *Int. J. Mod. Phys. A* **8** (1993) 4937 [hep-ph/9301281] [INSPIRE].

[10] I. Brivio et al., *Disentangling a dynamical Higgs*, *JHEP* **03** (2014) 024 [arXiv:1311.1823] [INSPIRE].

[11] R. Alonso, E.E. Jenkins and A.V. Manohar, *A Geometric Formulation of Higgs Effective Field Theory: Measuring the Curvature of Scalar Field Space*, *Phys. Lett. B* **754** (2016) 335 [arXiv:1511.00724] [INSPIRE].

[12] G. Buchalla, O. Catà, A. Celis and C. Krause, *Fitting Higgs Data with Nonlinear Effective Theory*, *Eur. Phys. J. C* **76** (2016) 233 [arXiv:1511.00988] [INSPIRE].

JHEP11(2021)173

[13] A. Helset, A. Martin and M. Trott, *The Geometric Standard Model Effective Field Theory*, *JHEP* **03** (2020) 163 [arXiv:2001.01453] [INSPIRE].

[14] T. Cohen, N. Craig, X. Lu and D. Sutherland, *Is SMEFT Enough?*, *JHEP* **03** (2021) 237 [arXiv:2008.08597] [INSPIRE].

[15] A. Alloul, B. Fuks and V. Sanz, *Phenomenology of the Higgs Effective Lagrangian via FEYNRULES*, *JHEP* **04** (2014) 110 [arXiv:1310.5150] [INSPIRE].

[16] P. Artoisenet et al., *A framework for Higgs characterisation*, *JHEP* **11** (2013) 043 [arXiv:1306.6464] [INSPIRE].

[17] R. Contino, M. Ghezzi, C. Grojean, M. Mühlleitner and M. Spira, *eHDECAY: an Implementation of the Higgs Effective Lagrangian into HDECAY*, *Comput. Phys. Commun.* **185** (2014) 3412 [arXiv:1403.3381] [INSPIRE].

[18] I. Brivio, Y. Jiang and M. Trott, *The SMEFTsim package, theory and tools*, *JHEP* **12** (2017) 070 [arXiv:1709.06492] [INSPIRE].

[19] J. De Blas et al., *HEPfit: a code for the combination of indirect and direct constraints on high energy physics models*, *Eur. Phys. J. C* **80** (2020) 456 [arXiv:1910.14012] [INSPIRE].

[20] C. Degrande, G. Durieux, F. Maltoni, K. Mimasu, E. Vryonidou and C. Zhang, *Automated one-loop computations in the standard model effective field theory*, *Phys. Rev. D* **103** (2021) 096024 [arXiv:2008.11743] [INSPIRE].

[21] T. Corbett, O.J.P. Eboli, J. Gonzalez-Fraile and M.C. Gonzalez-Garcia, *Robust Determination of the Higgs Couplings: Power to the Data*, *Phys. Rev. D* **87** (2013) 015022 [arXiv:1211.4580] [INSPIRE].

[22] R. Contino, M. Ghezzi, C. Grojean, M. Muhlleitner and M. Spira, *Effective Lagrangian for a light Higgs-like scalar*, *JHEP* **07** (2013) 035 [arXiv:1303.3876] [INSPIRE].

[23] A. Pomarol and F. Riva, *Towards the Ultimate SM Fit to Close in on Higgs Physics*, *JHEP* **01** (2014) 151 [arXiv:1308.2803] [INSPIRE].

[24] A. Falkowski and F. Riva, *Model-independent precision constraints on dimension-6 operators*, *JHEP* **02** (2015) 039 [arXiv:1411.0669] [INSPIRE].

[25] J. Ellis, V. Sanz and T. You, *The Effective Standard Model after LHC Run I*, *JHEP* **03** (2015) 157 [arXiv:1410.7703] [INSPIRE].

[26] J. Ellis, C.W. Murphy, V. Sanz and T. You, *Updated Global SMEFT Fit to Higgs, Diboson and Electroweak Data*, *JHEP* **06** (2018) 146 [arXiv:1803.03252] [INSPIRE].

[27] S. Dawson, S. Homiller and S.D. Lane, *Putting standard model EFT fits to work*, *Phys. Rev. D* **102** (2020) 055012 [arXiv:2007.01296] [INSPIRE].

[28] J. Ellis, M. Madigan, K. Mimasu, V. Sanz and T. You, *Top, Higgs, Diboson and Electroweak Fit to the Standard Model Effective Field Theory*, *JHEP* **04** (2021) 279 [arXiv:2012.02779] [INSPIRE].

[29] SMEFiT collaboration, *Combined SMEFT interpretation of Higgs, diboson, and top quark data from the LHC*, *JHEP* **11** (2021) 089 [arXiv:2105.00006] [INSPIRE].

[30] G. Passarino, *NLO Inspired Effective Lagrangians for Higgs Physics*, *Nucl. Phys. B* **868** (2013) 416 [arXiv:1209.5538] [INSPIRE].

JHEP11(2021)173

[31] ATLAS collaboration, *Combined measurement of differential and total cross sections in the $H \to \gamma\gamma$ and the $H \to ZZ^* \to 4\ell$ decay channels at $\sqrt{s} = 13$ TeV with the ATLAS detector*, *Phys. Lett. B* **786** (2018) 114 [arXiv:1805.10197] [INSPIRE].

[32] CMS collaboration, *Measurement and interpretation of differential cross sections for Higgs boson production at $\sqrt{s} = 13$ TeV*, *Phys. Lett. B* **792** (2019) 369 [arXiv:1812.06504] [INSPIRE].

[33] ATLAS collaboration, *Measurements of Higgs boson properties in the diphoton decay channel with 36 fb^{-1} of pp collision data at $\sqrt{s} = 13$ TeV with the ATLAS detector*, *Phys. Rev. D* **98** (2018) 052005 [arXiv:1802.04146] [INSPIRE].

[34] ATLAS collaboration, *Measurements of the Higgs boson inclusive and differential fiducial cross sections in the 4ℓ decay channel at $\sqrt{s} = 13$ TeV*, *Eur. Phys. J. C* **80** (2020) 942 [arXiv:2004.03969] [INSPIRE].

[35] CMS collaboration, *Inclusive search for highly boosted Higgs bosons decaying to bottom quark-antiquark pairs in proton-proton collisions at $\sqrt{s} = 13$ TeV*, *JHEP* **12** (2020) 085 [arXiv:2006.13251] [INSPIRE].

[36] ATLAS collaboration, *Identification of boosted Higgs bosons decaying into b-quark pairs with the ATLAS detector at 13 TeV*, *Eur. Phys. J. C* **79** (2019) 836 [arXiv:1906.11005] [INSPIRE].

[37] ATLAS collaboration, *Study of Higgs-boson production with large transverse momentum using the $H \to b\bar{b}$ decay with the ATLAS detector*, ATLAS-CONF-2021-010 (2021).

[38] CMS collaboration, *Sensitivity projections for Higgs boson properties measurements at the HL-LHC*, CMS-PAS-FTR-18-011 (2018).

[39] ATLAS collaboration, *Prospects for differential cross-section measurements of Higgs boson production measured in decays to ZZ and $\gamma\gamma$ with the ATLAS experiment at the High-Luminosity LHC*, ATL-PHYS-PUB-2018-040 (2018).

[40] R.K. Ellis, I. Hinchliffe, M. Soldate and J.J. van der Bij, *Higgs Decay to $\tau^+ \tau^-$: A Possible Signature of Intermediate Mass Higgs Bosons at the SSC*, *Nucl. Phys. B* **297** (1988) 221 [INSPIRE].

[41] U. Baur and E.W.N. Glover, *Higgs Boson Production at Large Transverse Momentum in Hadronic Collisions*, *Nucl. Phys. B* **339** (1990) 38 [INSPIRE].

[42] C.R. Schmidt, *$H \to ggg(gq\bar{q})$ at two loops in the large-M_t limit*, *Phys. Lett. B* **413** (1997) 391 [hep-ph/9707448] [INSPIRE].

[43] D. de Florian, M. Grazzini and Z. Kunszt, *Higgs production with large transverse momentum in hadronic collisions at next-to-leading order*, *Phys. Rev. Lett.* **82** (1999) 5209 [hep-ph/9902483] [INSPIRE].

[44] C.J. Glosser and C.R. Schmidt, *Next-to-leading corrections to the Higgs boson transverse momentum spectrum in gluon fusion*, *JHEP* **12** (2002) 016 [hep-ph/0209248] [INSPIRE].

[45] V. Ravindran, J. Smith and W.L. Van Neerven, *Next-to-leading order QCD corrections to differential distributions of Higgs boson production in hadron hadron collisions*, *Nucl. Phys. B* **634** (2002) 247 [hep-ph/0201114] [INSPIRE].

[46] R.V. Harlander, T. Neumann, K.J. Ozeren and M. Wiesemann, *Top-mass effects in differential Higgs production through gluon fusion at order $\mathcal{O}(\alpha_s^4)$*, *JHEP* **08** (2012) 139 [arXiv:1206.0157] [INSPIRE].

JHEP11(2021)173

[47] T. Neumann and M. Wiesemann, *Finite top-mass effects in gluon-induced Higgs production with a jet-veto at NNLO*, *JHEP* **11** (2014) 150 [arXiv:1408.6836] [INSPIRE].

[48] T. Neumann and C. Williams, *The Higgs boson at high p_T*, *Phys. Rev. D* **95** (2017) 014004 [arXiv:1609.00367] [INSPIRE].

[49] R. Frederix, S. Frixione, E. Vryonidou and M. Wiesemann, *Heavy-quark mass effects in Higgs plus jets production*, *JHEP* **08** (2016) 006 [arXiv:1604.03017] [INSPIRE].

[50] J.M. Lindert, K. Kudashkin, K. Melnikov and C. Wever, *Higgs bosons with large transverse momentum at the LHC*, *Phys. Lett. B* **782** (2018) 210 [arXiv:1801.08226] [INSPIRE].

[51] T. Neumann, *NLO Higgs+jet production at large transverse momenta including top quark mass effects*, *J. Phys. Comm.* **2** (2018) 095017 [arXiv:1802.02981] [INSPIRE].

[52] S.P. Jones, M. Kerner and G. Luisoni, *Next-to-Leading-Order QCD Corrections to Higgs Boson Plus Jet Production with Full Top-Quark Mass Dependence*, *Phys. Rev. Lett.* **120** (2018) 162001 [arXiv:1802.00349] [INSPIRE].

[53] R. Boughezal, F. Caola, K. Melnikov, F. Petriello and M. Schulze, *Higgs boson production in association with a jet at next-to-next-to-leading order*, *Phys. Rev. Lett.* **115** (2015) 082003 [arXiv:1504.07922] [INSPIRE].

[54] R. Boughezal, C. Focke, W. Giele, X. Liu and F. Petriello, *Higgs boson production in association with a jet at NNLO using jettiness subtraction*, *Phys. Lett. B* **748** (2015) 5 [arXiv:1505.03893] [INSPIRE].

[55] X. Chen, J. Cruz-Martinez, T. Gehrmann, E.W.N. Glover and M. Jaquier, *NNLO QCD corrections to Higgs boson production at large transverse momentum*, *JHEP* **10** (2016) 066 [arXiv:1607.08817] [INSPIRE].

[56] K. Becker et al., *Precise predictions for boosted Higgs production*, arXiv:2005.07762 [INSPIRE].

[57] S. Alioli, P. Nason, C. Oleari and E. Re, *NLO Higgs boson production via gluon fusion matched with shower in POWHEG*, *JHEP* **04** (2009) 002 [arXiv:0812.0578] [INSPIRE].

[58] J.M. Campbell, R.K. Ellis, R. Frederix, P. Nason, C. Oleari and C. Williams, *NLO Higgs Boson Production Plus One and Two Jets Using the POWHEG BOX, MadGraph4 and MCFM*, *JHEP* **07** (2012) 092 [arXiv:1202.5475] [INSPIRE].

[59] K. Hamilton, P. Nason, C. Oleari and G. Zanderighi, *Merging H/W/Z + 0 and 1 jet at NLO with no merging scale: a path to parton shower + NNLO matching*, *JHEP* **05** (2013) 082 [arXiv:1212.4504] [INSPIRE].

[60] A. Azatov and A. Paul, *Probing Higgs couplings with high p_T Higgs production*, *JHEP* **01** (2014) 014 [arXiv:1309.5273] [INSPIRE].

[61] C. Grojean, E. Salvioni, M. Schlaffer and A. Weiler, *Very boosted Higgs in gluon fusion*, *JHEP* **05** (2014) 022 [arXiv:1312.3317] [INSPIRE].

[62] U. Langenegger, M. Spira and I. Strebel, *Testing the Higgs Boson Coupling to Gluons*, arXiv:1507.01373 [INSPIRE].

[63] F. Maltoni, E. Vryonidou and C. Zhang, *Higgs production in association with a top-antitop pair in the Standard Model Effective Field Theory at NLO in QCD*, *JHEP* **10** (2016) 123 [arXiv:1607.05330] [INSPIRE].

JHEP11(2021)173

[64] N. Deutschmann, C. Duhr, F. Maltoni and E. Vryonidou, *Gluon-fusion Higgs production in the Standard Model Effective Field Theory*, *JHEP* **12** (2017) 063 [*Erratum ibid.* **02** (2018) 159] [arXiv:1708.00460] [INSPIRE].

[65] M. Grazzini, A. Ilnicka, M. Spira and M. Wiesemann, *Modeling BSM effects on the Higgs transverse-momentum spectrum in an EFT approach*, *JHEP* **03** (2017) 115 [arXiv:1612.00283] [INSPIRE].

[66] M. Grazzini, A. Ilnicka and M. Spira, *Higgs boson production at large transverse momentum within the SMEFT: analytical results*, *Eur. Phys. J. C* **78** (2018) 808 [arXiv:1806.08832] [INSPIRE].

[67] R.V. Harlander and T. Neumann, *Probing the nature of the Higgs-gluon coupling*, *Phys. Rev. D* **88** (2013) 074015 [arXiv:1308.2225] [INSPIRE].

[68] S. Dawson, I.M. Lewis and M. Zeng, *Effective field theory for Higgs boson plus jet production*, *Phys. Rev. D* **90** (2014) 093007 [arXiv:1409.6299] [INSPIRE].

[69] M. Buschmann et al., *Mass effects in the Higgs-gluon coupling: boosted vs off-shell production*, *JHEP* **02** (2015) 038 [arXiv:1410.5806] [INSPIRE].

[70] R. Mammen Abraham et al., *Directly Probing the Higgs-top Coupling at High Scales*, arXiv:2106.00018 [INSPIRE].

[71] I. Brivio et al., *O new physics, where art thou? A global search in the top sector*, *JHEP* **02** (2020) 131 [arXiv:1910.03606] [INSPIRE].

[72] E.E. Jenkins, A.V. Manohar and M. Trott, *Renormalization Group Evolution of the Standard Model Dimension Six Operators I: Formalism and lambda Dependence*, *JHEP* **10** (2013) 087 [arXiv:1308.2627] [INSPIRE].

[73] E.E. Jenkins, A.V. Manohar and M. Trott, *Renormalization Group Evolution of the Standard Model Dimension Six Operators II: Yukawa Dependence*, *JHEP* **01** (2014) 035 [arXiv:1310.4838] [INSPIRE].

[74] R. Alonso, E.E. Jenkins, A.V. Manohar and M. Trott, *Renormalization Group Evolution of the Standard Model Dimension Six Operators III: Gauge Coupling Dependence and Phenomenology*, *JHEP* **04** (2014) 159 [arXiv:1312.2014] [INSPIRE].

[75] S. Dittmaier, M. Krämer and M. Spira, *Higgs radiation off bottom quarks at the Tevatron and the CERN LHC*, *Phys. Rev. D* **70** (2004) 074010 [hep-ph/0309204] [INSPIRE].

[76] S. Dawson, C.B. Jackson, L. Reina and D. Wackeroth, *Exclusive Higgs boson production with bottom quarks at hadron colliders*, *Phys. Rev. D* **69** (2004) 074027 [hep-ph/0311067] [INSPIRE].

[77] R. Harlander and M. Wiesemann, *Jet-veto in bottom-quark induced Higgs production at next-to-next-to-leading order*, *JHEP* **04** (2012) 066 [arXiv:1111.2182] [INSPIRE].

[78] R.V. Harlander, K.J. Ozeren and M. Wiesemann, *Higgs plus jet production in bottom quark annihilation at next-to-leading order*, *Phys. Lett. B* **693** (2010) 269 [arXiv:1007.5411] [INSPIRE].

[79] M. Wiesemann, R. Frederix, S. Frixione, V. Hirschi, F. Maltoni and P. Torrielli, *Higgs production in association with bottom quarks*, *JHEP* **02** (2015) 132 [arXiv:1409.5301] [INSPIRE].

JHEP11(2021)173

[80] R.V. Harlander, A. Tripathi and M. Wiesemann, *Higgs production in bottom quark annihilation: Transverse momentum distribution at NNLO+NNLL*, *Phys. Rev. D* **90** (2014) 015017 [arXiv:1403.7196] [INSPIRE].

[81] N. Deutschmann, F. Maltoni, M. Wiesemann and M. Zaro, *Top-Yukawa contributions to bbH production at the LHC*, *JHEP* **07** (2019) 054 [arXiv:1808.01660] [INSPIRE].

[82] H. Mantler and M. Wiesemann, *Top- and bottom-mass effects in hadronic Higgs production at small transverse momenta through LO+NLL*, *Eur. Phys. J. C* **73** (2013) 2467 [arXiv:1210.8263] [INSPIRE].

[83] R.V. Harlander, H. Mantler and M. Wiesemann, *Transverse momentum resummation for Higgs production via gluon fusion in the MSSM*, *JHEP* **11** (2014) 116 [arXiv:1409.0531] [INSPIRE].

[84] S. Liebler, H. Mantler and M. Wiesemann, *Distributions for neutral Higgs production in the NMSSM*, arXiv:1608.02949 [INSPIRE].

[85] G. Bozzi, S. Catani, D. de Florian and M. Grazzini, *Transverse-momentum resummation and the spectrum of the Higgs boson at the LHC*, *Nucl. Phys. B* **737** (2006) 73 [hep-ph/0508068] [INSPIRE].

[86] D. de Florian, G. Ferrera, M. Grazzini and D. Tommasini, *Transverse-momentum resummation: Higgs boson production at the Tevatron and the LHC*, *JHEP* **11** (2011) 064 [arXiv:1109.2109] [INSPIRE].

[87] LHC Higgs Cross Section Working Group collaboration, *Handbook of LHC Higgs Cross Sections: 4. Deciphering the Nature of the Higgs Sector*, arXiv:1610.07922 [INSPIRE].

[88] P. Marquard, A.V. Smirnov, V.A. Smirnov, M. Steinhauser and D. Wellmann, $\overline{\text{MS}}$*-on-shell quark mass relation up to four loops in QCD and a general* SU(N) *gauge group*, *Phys. Rev. D* **94** (2016) 074025 [arXiv:1606.06754] [INSPIRE].

[89] K.G. Chetyrkin, *Quark mass anomalous dimension to* $O(\alpha_S^4)$, *Phys. Lett. B* **404** (1997) 161 [hep-ph/9703278] [INSPIRE].

[90] J.A.M. Vermaseren, S.A. Larin and T. van Ritbergen, *The four loop quark mass anomalous dimension and the invariant quark mass*, *Phys. Lett. B* **405** (1997) 327 [hep-ph/9703284] [INSPIRE].

[91] J. Alwall et al., *The automated computation of tree-level and next-to-leading order differential cross sections, and their matching to parton shower simulations*, *JHEP* **07** (2014) 079 [arXiv:1405.0301] [INSPIRE].

[92] D. Buarque Franzosi and C. Zhang, *Probing the top-quark chromomagnetic dipole moment at next-to-leading order in QCD*, *Phys. Rev. D* **91** (2015) 114010 [arXiv:1503.08841] [INSPIRE].

[93] J. Butterworth et al., *PDF4LHC recommendations for LHC Run II*, *J. Phys. G* **43** (2016) 023001 [arXiv:1510.03865] [INSPIRE].

[94] NNPDF collaboration, *Parton distributions for the LHC Run II*, *JHEP* **04** (2015) 040 [arXiv:1410.8849] [INSPIRE].

[95] S. Dulat et al., *New parton distribution functions from a global analysis of quantum chromodynamics*, *Phys. Rev. D* **93** (2016) 033006 [arXiv:1506.07443] [INSPIRE].

JHEP11(2021)173

[96] L.A. Harland-Lang, A.D. Martin, P. Motylinski and R.S. Thorne, *Parton distributions in the LHC era: MMHT 2014 PDFs*, *Eur. Phys. J. C* **75** (2015) 204 [arXiv:1412.3989] [INSPIRE].

[97] J. Gao and P. Nadolsky, *A meta-analysis of parton distribution functions*, *JHEP* **07** (2014) 035 [arXiv:1401.0013] [INSPIRE].

[98] S. Carrazza, S. Forte, Z. Kassabov, J.I. Latorre and J. Rojo, *An Unbiased Hessian Representation for Monte Carlo PDFs*, *Eur. Phys. J. C* **75** (2015) 369 [arXiv:1505.06736] [INSPIRE].

[99] R. Brun and F. Rademakers, *ROOT: An object oriented data analysis framework*, *Nucl. Instrum. Meth. A* **389** (1997) 81 [INSPIRE].

[100] F. James and M. Roos, *Minuit: A System for Function Minimization and Analysis of the Parameter Errors and Correlations*, *Comput. Phys. Commun.* **10** (1975) 343 [INSPIRE].

[101] J. Baglio, S. Dawson, S. Homiller, S.D. Lane and I.M. Lewis, *Validity of SMEFT studies of VH and VV production at NLO*, *Phys. Rev. D* **101** (2020) 115004 [arXiv:2003.07862] [INSPIRE].

[102] F. del Aguila, M. Pérez-Victoria and J. Santiago, *Observable contributions of new exotic quarks to quark mixing*, *JHEP* **09** (2000) 011 [hep-ph/0007316] [INSPIRE].

[103] ATLAS collaboration, *Combination of the searches for pair-produced vector-like partners of the third-generation quarks at $\sqrt{s} = 13$ TeV with the ATLAS detector*, *Phys. Rev. Lett.* **121** (2018) 211801 [arXiv:1808.02343] [INSPIRE].

[104] J.A. Aguilar-Saavedra, R. Benbrik, S. Heinemeyer and M. Pérez-Victoria, *Handbook of vectorlike quarks: Mixing and single production*, *Phys. Rev. D* **88** (2013) 094010 [arXiv:1306.0572] [INSPIRE].

[105] M.E. Peskin and T. Takeuchi, *A New constraint on a strongly interacting Higgs sector*, *Phys. Rev. Lett.* **65** (1990) 964 [INSPIRE].

[106] A. Banfi, A. Martin and V. Sanz, *Probing top-partners in Higgs+jets*, *JHEP* **08** (2014) 053 [arXiv:1308.4771] [INSPIRE].

[107] A. Banfi, A. Bond, A. Martin and V. Sanz, *Digging for Top Squarks from Higgs data: from signal strengths to differential distributions*, *JHEP* **11** (2018) 171 [arXiv:1806.05598] [INSPIRE].

[108] CMS collaboration, *Combined searches for the production of supersymmetric top quark partners in proton–proton collisions at $\sqrt{s} = 13$ TeV*, *Eur. Phys. J. C* **81** (2021) 970 [arXiv:2107.10892] [INSPIRE].

[109] ATLAS collaboration, *SUSY Summary Plots June 2021*, ATL-PHYS-PUB-2021-019 (2021).

[110] B. Allanach, *Softsusy: A program for calculating supersymmetric spectra*, *Comput. Phys. Commun.* **143** (2002) 305.

[111] R.V. Harlander, S. Liebler and H. Mantler, *Sushi: A program for the calculation of Higgs production in gluon fusion and bottom-quark annihilation in the standard model and the MSSM*, *Comput. Phys. Commun.* **184** (2013) 1605 [arXiv:1212.3249] [INSPIRE].

[112] C. Zhang and S. Willenbrock, *Effective-Field-Theory Approach to Top-Quark Production and Decay*, *Phys. Rev. D* **83** (2011) 034006 [arXiv:1008.3869] [INSPIRE].

JHEP11(2021)173

[113] CMS collaboration, *Measurements of $\mathrm{t\bar{t}}$ differential cross sections in proton-proton collisions at $\sqrt{s} = 13$ TeV using events containing two leptons*, *JHEP* **02** (2019) 149 [arXiv:1811.06625] [INSPIRE].

[114] CMS collaboration, *Search for new physics in top quark production with additional leptons in proton-proton collisions at $\sqrt{s} = 13$ TeV using effective field theory*, *JHEP* **03** (2021) 095 [arXiv:2012.04120] [INSPIRE].

[115] ATLAS collaboration, *Measurement of the associated production of a Higgs boson decaying into b-quarks with a vector boson at high transverse momentum in pp collisions at $\sqrt{s} = 13$ TeV with the ATLAS detector*, *Phys. Lett. B* **816** (2021) 136204 [arXiv:2008.02508] [INSPIRE].

[116] CMS collaboration, *Measurements of production cross sections of the Higgs boson in the four-lepton final state in proton-proton collisions at $\sqrt{s} = 13$ TeV*, *Eur. Phys. J. C* **81** (2021) 488 [arXiv:2103.04956] [INSPIRE].

[117] ATLAS collaboration, *Combined measurement of the total and differential cross sections in the $H \to \gamma\gamma$ and the $H \to ZZ^* \to 4\ell$ decay channels at $\sqrt{s} = 13$ TeV with the ATLAS detector*, ATLAS-CONF-2019-032, (2019).

[118] CMS collaboration, *Sensitivity projections for Higgs boson properties measurements at the HL-LHC*, CMS-PAS-FTR-18-011 (2018).

[119] ATLAS collaboration, *A combination of measurements of Higgs boson production and decay using up to 139 fb^{-1} of proton–proton collision data at $\sqrt{s} = 13$ TeV collected with the ATLAS experiment*, ATLAS-CONF-2020-027 (2020).

[120] CMS collaboration, *Combined Higgs boson production and decay measurements with up to 137 fb^{-1} of proton-proton collision data at $\sqrt{s} = 13$ TeV*, CMS-PAS-HIG-19-005 (2019).

[121] LHC Higgs Cross Section Working Group collaboration, *Handbook of LHC Higgs Cross Sections: 3. Higgs Properties*, arXiv:1307.1347 [INSPIRE].

[122] CMS collaboration, *Measurement and interpretation of differential cross sections for Higgs boson production at $\sqrt{s} = 13$ TeV*, *Phys. Lett. B* **792** (2019) 369 [arXiv:1812.06504] [INSPIRE].

[123] ATLAS collaboration, *Interpretations of the combined measurement of Higgs boson production and decay*, ATLAS-CONF-2020-053 (2020).

[124] C.G. Callan, Jr., *Broken scale invariance in scalar field theory*, *Phys. Rev. D* **2** (1970) 1541 [INSPIRE].

[125] K. Symanzik, *Small distance behavior in field theory and power counting*, *Commun. Math. Phys.* **18** (1970) 227 [INSPIRE].

[126] S.R. Coleman and R. Jackiw, *Why dilatation generators do not generate dilatations?*, *Annals Phys.* **67** (1971) 552 [INSPIRE].

[127] R.J. Crewther, *Nonperturbative evaluation of the anomalies in low-energy theorems*, *Phys. Rev. Lett.* **28** (1972) 1421 [INSPIRE].

[128] M.S. Chanowitz and J.R. Ellis, *Canonical Anomalies and Broken Scale Invariance*, *Phys. Lett. B* **40** (1972) 397 [INSPIRE].

[129] M.S. Chanowitz and J.R. Ellis, *Canonical Trace Anomalies*, *Phys. Rev. D* **7** (1973) 2490 [INSPIRE].

JHEP11(2021)173